

# Comparison of DECam engineering CCDs with the DES technical requirements

T. Abbott<sup>2</sup>, B. Angstadt<sup>3</sup>, J. Campa<sup>4</sup>, H. Cease<sup>3</sup>, G. Derylo<sup>3</sup>, H.T. Diehl<sup>3</sup>, J. Estrada<sup>3</sup>, B. Flaugher<sup>3</sup>, D. Kubik<sup>3</sup>, K. Kuk<sup>3</sup>, S. Kuhlman<sup>1</sup>, H. Lin<sup>3</sup>, A. Plazas<sup>3,5</sup>, R. Schmidt<sup>2</sup>, V. Scarpine<sup>3</sup>, K. Schultz<sup>3</sup>, T. Shaw<sup>3</sup>, W. Stuermer<sup>3</sup>, D. Thompson<sup>6</sup>

<sup>1</sup> *Argonne National Laboratory, Argonne, Illinois, U.S.A*

<sup>2</sup> *Cerro Tololo Inter-American Observatory, La Serena, Chile*

<sup>3</sup> *Fermi National Accelerator Laboratory, Batavia, Illinois, U.S.A.*

<sup>4</sup> *IECC/IFAE, Barcelona, Spain*

<sup>5</sup> *Universidad de Los Andes, Bogota, Colombia*

<sup>6</sup> *University of Chicago, Chicago, Illinois, U.S.A.*

(Dated: April 27, 2007)

## Abstract

The document describes how the performance of the engineering grade CCDs for DECam compares with the technical requirements for the Dark Energy Survey. Detailed performance measurements are presented for a few detectors. This document also describes the procedure by which the technical requirements will be compared with DECam CCDs during production. The results indicate that we can satisfy every technical requirement with the engineering grade detectors. This document is not an extensive description of the tests done on every device packaged.

## Contents

<b>I. Introduction</b>	3
<b>II. Nonlinearity and Full Well (T-10 and T-11)</b>	3
<b>III. Residual Image (T-12)</b>	4
<b>IV. Readout rate and Noise (T-13 and T-25)</b>	6
<b>V. Charge transfer inefficiency (T-14)</b>	8
<b>VI. Quantum Efficiency (T-20 ,T-21 and T-23)</b>	13
A. Absolute QE (T-20)	13
B. QE stability (T-21)	16
C. QE uniformity (T-23)	19
<b>VII. Charge Diffusion (T-27)</b>	20
<b>VIII. Flatness (T-28 and T-29)</b>	24
<b>IX. Cosmetic defects (T-30)</b>	26
Traps	27
<b>X. Dark Current (TP-1)</b>	28
<b>XI. Crosstalk (TP-2)</b>	29
<b>XII. Plan for production CCD testing</b>	29
<b>Stage 1 testing</b>	29
<b>Stage 2 testing</b>	31
<b>Stage 3 testing</b>	32
<b>References</b>	32

## I. INTRODUCTION

The technical requirements for the Dark Energy Survey [1] [2] are discussed in Ref [4]. In most cases they correspond to standard requirements for CCDs, except for the higher quantum efficiency in the red part of the visible range, QE [“z”] > 65%, for the SDSS “z” filter, achieved using 250  $\mu\text{m}$  thick CCDs developed at LBNL [3]. A summary for the technical requirements for the focal plane CCD is presented in Table I.

In this document we present studies done for engineering DECam CCDs (Lot 1A and Lot 1B) and compare the performance of these devices with the technical requirements in Table I. Unless otherwise specified the results shown correspond to pb-22-01, a 2k x 2k CCD, 250  $\mu\text{m}$  thick, packaged in a picture frame. The tests are done at an operating temperature of 173 K, using the bias and clock voltages presented in Table II.

During DES production CCD testing we plan to test up to 5 CCDs a week. Towards the end of this document we discuss our plans to check the technical requirements on every DES CCD during production.

## II. NONLINEARITY AND FULL WELL (T-10 AND T-11)

The full well capacity of the CCD is measured as the charge level at which the CCD starts to show a deviation from linearity of more than 1%. For this reason T-10 and T-11 are related requirements.

The measurement is done by taking a set of exposures with varying exposure time, recording the signal level as a function of exposure time. An example of such a study is shown in Fig. 1. In this case the data was collected with a gain setting selected to match the dynamic range of the readout electronics to  $\approx 130000e$ . The plot shows the number of electrons as a function of exposure time and a linear fit to the data (red line). The relative residuals to the fit are shown in Fig. 2 and are between  $\pm 1\%$  for charge levels  $\leq 130000e$ . We therefore conclude that this CCD satisfies our technical requirements T-10 and T-11 from Table I.

It should be noted that the electronic gain selected for this test is such that we did not probe where the CCD starts to show a nonlinearity larger than 1%.

	measurement	specification
T-10	nonlinearity	$< 1 \%$
T-11	full well	$> 130000 \text{ e-}$
T-12	residual image	$< 10 \text{ e-}$ from $3 \times 10^6 \text{ e-}$ spread over 5 pixels
T-13	readout rate	250 kpix/s
T-14	CTI	$< 10^{-5}$
T-20	QE [g, r, i, z]	[60%, 75%, 70%, 65%]
T-21	QE instability	$\leq 0.3\%$ in 12-18 hours
T-23	QE uniformity in focal plane	$\leq 5\%$ in 12-18 hours
T-25	readout noise	$\leq 15 \text{ e-/pix}$
T-27	charge diffusion	1-D $\sigma < 7.5 \mu\text{m}$
T-28	flatness $1 \text{ cm}^2$ region	$< 3 \mu\text{m}$ r.m.s. in deviation from flat
T-29	flatness between T-28 regions	$< 10 \mu\text{m}$ deviation
T-30	cosmetic defects	$< 5 \%$ loss from non-usable pixels
TP-1	dark current	$< \text{dark current } 25 \text{ e/pix/hour}$
TP-2	crosstalk	$< 10^{-3}$

TABLE I: Technical specs for the DES CCDs [4]. TP-1 and TP-2 are preliminary technical requirements not yet included in Ref. [4].

### III. RESIDUAL IMAGE (T-12)

Residual image is produced by charge accumulated on the detector pixels that is produced by a remnant of a previous exposures. Is typically seen in dark exposures taken after an exposure where significant light had been collected. The problem of residual image on a CCD is usually avoided by operating the detector with inversion in the vertical clocks, see Ref. [5] for details on this topic. To achieve full depletion in  $250 \mu\text{m}$ , these CCDs are operated with a substrate voltage  $V_{SUB} = 40 \text{ V}$  and for that reason, the DECam detectors cannot be operated in inversion mode [5]. This means that if nothing is done, there could be a significant residual image on these detectors. An example of a residual image produced after a fully saturated exposure is shown in Fig. 3.

In order to eliminate the residual image in these detectors, the CCD is briefly set into

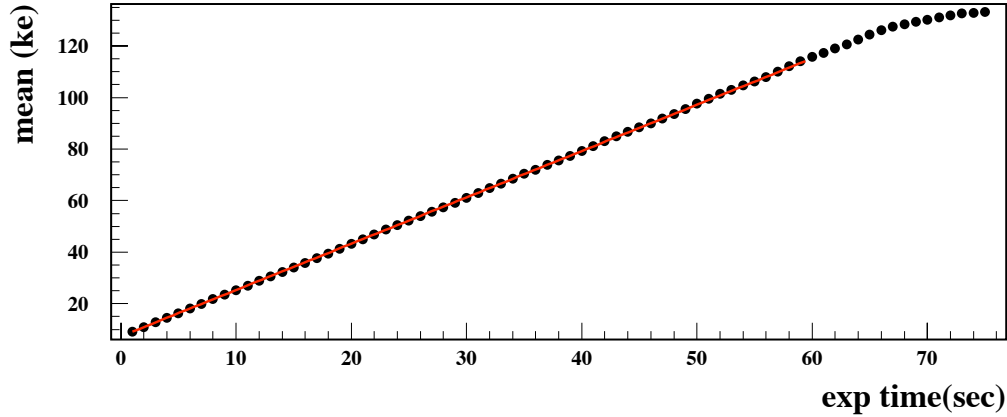


FIG. 1: Charge collected in the CCD as a function of exposure time. The red curve is a linear fit used to measure nonlinearity. The electronic gain and the pedestals are set to reach the maximum of the dynamic range for 1300000 e.

inversion for the vertical clocks between exposures. This is done in the following sequence which we call ERASE (taking a total of 0.6 s) :

1. substrate voltage is lowered to  $V_{sub} = 0V$  in a ramp : 20 steps with 0.001 s delay between steps
2. vertical clocks are raised to 8 V : kept high for 0.5 s
3. substrate voltage is raised back to the operating level  $V_{sub} = 40 V$  with a ramp: 20 steps with 0.001 s delay between steps
4. clear to get the CCD ready for a new exposure.

The efficiency of the ERASE mechanism to eliminate the residual image has been studied by producing a fully saturate, flat field image with more than  $3 \times 10^6$  e per pixel, followed by a series of 400-second dark exposures for a couple of hours. The results are shown in Fig. 4. The plot shows that in the case where the ERASE is used, the readout goes back to the dark level of 10 e/pix/hour for the next exposure after the saturation. When the ERASE is not used the persistence of the saturation is still noticeable many hours later. When the ERASE

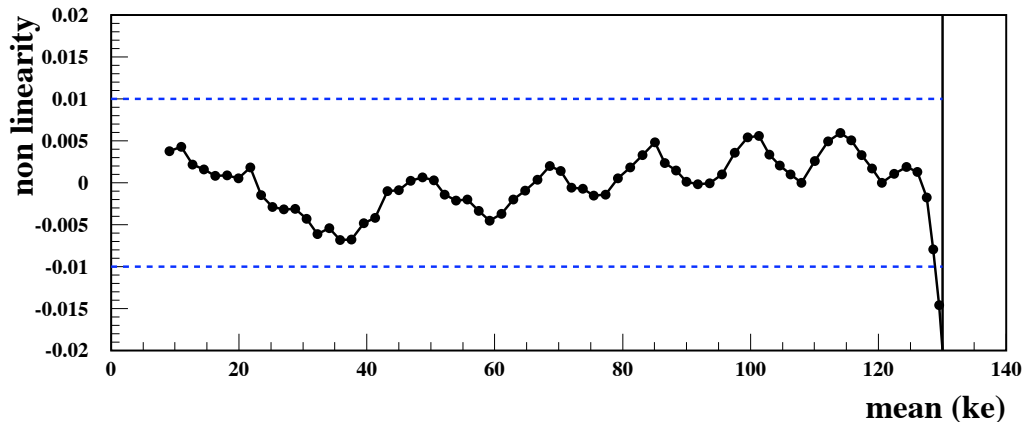


FIG. 2: Relative residuals as a function of charge (kilo-electrons). The CCD has better than 1% linearity up to 130000e. T-10 and T-11 from Table I are satisfied.

is used, residual image is then less than 1 e/h for a signal level of  $3 \times 10^6$  e; the plot in Fig. 4 shows no evidence for a residual image. Considering that the longer exposures planned for DES are of 400 sec, we conclude that the detector satisfies the technical requirement T-12 presented in Table I.

#### IV. READOUT RATE AND NOISE (T-13 AND T-25)

For the DECam instrument we will use electronics based on the Monsoon[12] standard developed by NOAO (all the tests presented here are done using the Monsoon electronics). The readout is done by a correlated double sample (CDS) [5] measurement of the video output. The noise in the detectors is measured by producing an image and looking at the RMS in the serial overscan. The gain is determined by a photon transfer curve [5] (the noise can then be expressed in terms of electrons).

In this section we present the performance of a picture frame CCD with a source follower circuit mounted approximately  $\approx 2$  cm away from the CCD (inside the dewar). The video signal travels  $\approx 35$  cm over a microcoax cable to a preamplifier board outside the dewar. The signal is then travels  $\approx 1.5$  m over a shielded cable to the readout electronics.

From the clocking sequence required to readout the CCDs, we have identified a strong

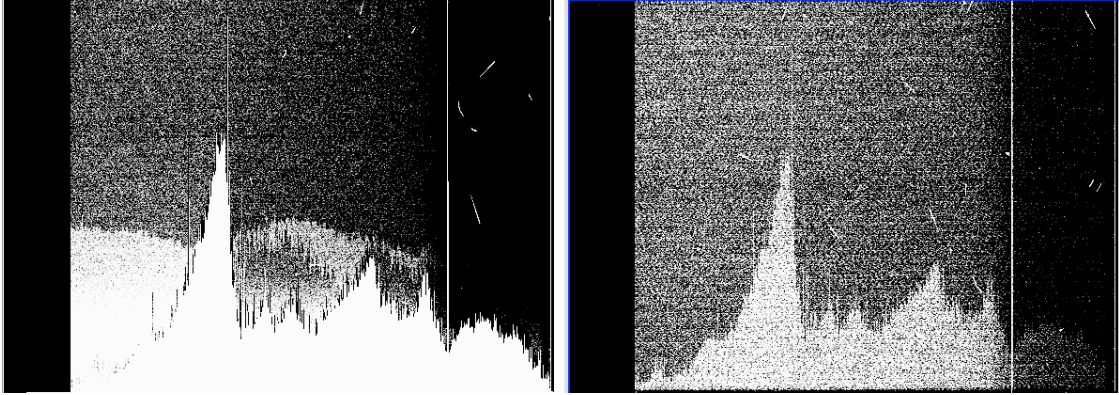


FIG. 3: Example of a residual image observed on our device after a saturated exposure produced with a flat illumination more than  $3 \times 10^6$ e per pixel. The panel on the left shows the exposure immediately after the saturation. Even after a full readout has been done, the serial register is saturated and charge moves from it to the active region of the detector. The panel on the right corresponds to a readout performed 7 minutes after the saturation. The serial register is not saturating anymore, but it is still possible to see the imprint of the saturation produced earlier. The “skyline” structure near the bottom of the image is a residual image.

dependence of the noise in two delays. The noise is very strongly dependent on the width of the integration window (= dwell time or “slope”) and the separation between the two integration windows used for CDS (an example of an oscilloscope trace with the video signal and the CDS integration windows is presented in Fig.32 ). We study the noise as a function of these two delays. The results for noise as a function of these delays are presented in Fig.5 and Fig.6. We have not yet optimized our default readout times according to the results obtained in these studies. Most of the data collected so far in the DES CCD testing effort used the slower readout marked with an arrow in Fig.5.

The relevant specification (T-25) requires  $\sigma \leq 15e^-$  for a readout speed of 250 kpix/sec (corresponding to  $4 \mu\text{s}$  per pixel). The results presented in Fig.5 show that we can achieve the specification with two different configurations, given by  $[\text{integ}, \text{SW}] = [3, 3]$  and  $[\text{integ}, \text{SW}] = [2, 5]$ . However, considering that the environment at the telescope will be very different (and probably noisier for the electronics) with respect to the lab we would like to meet the more aggressive goal of  $\sigma \leq 10 e^-$  at the same readout speed. The more ambitious goal is achieved consistently at a readout speed of  $4.8 \mu\text{s}$ , corresponding to 83% of the readout speed goal.

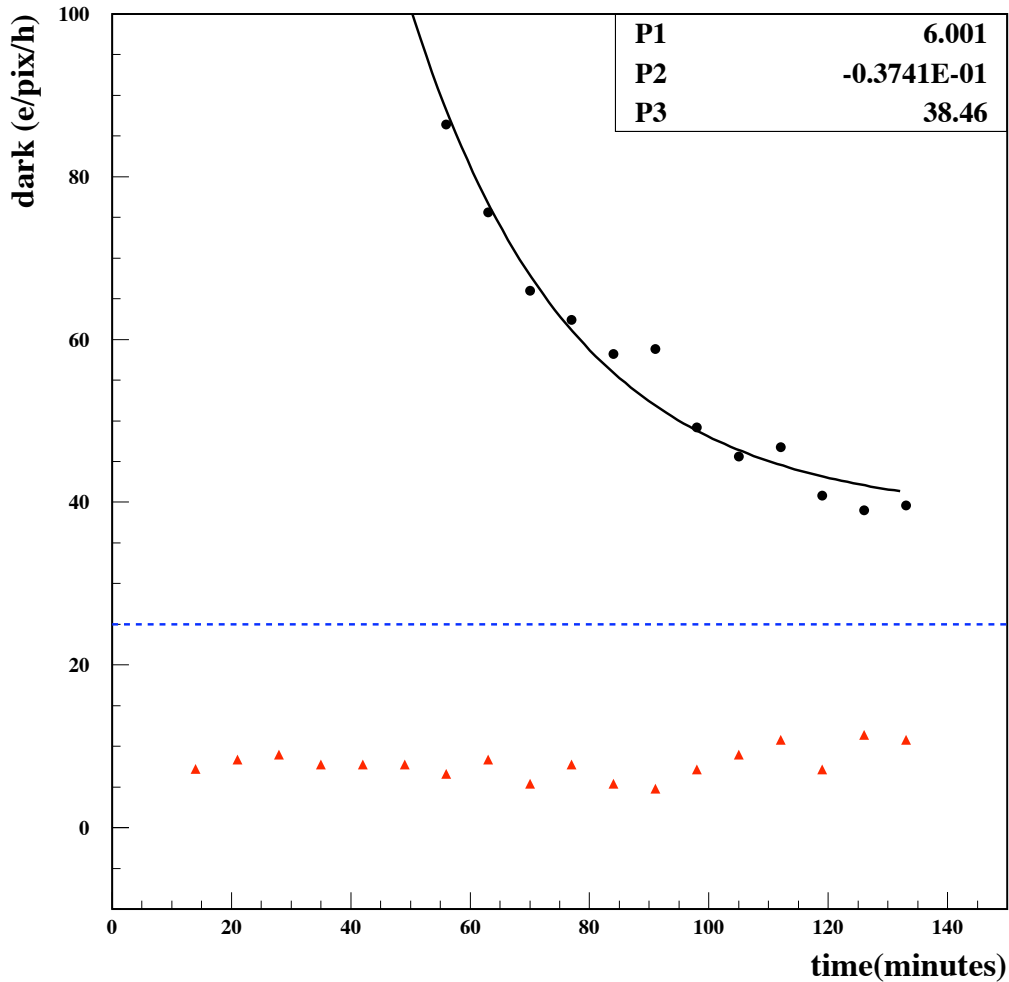


FIG. 4: Average signal level measured in dark exposures taken after a fully saturated flat image is produced with more than  $3 \times 10^6$ e per pixel at  $T = 0$  minutes (origin in the  $x$ -axis. The black circles correspond to the images obtained without using the ERASE mechanism. The red triangles correspond to the images collected when an ERASE is performed after the saturation.

## V. CHARGE TRANSFER INEFFICIENCY (T-14)

The method used to calculate the overall charge transfer inefficiency (CTI) is the so-called extended pixel edge response (EPER). The CCD is illuminated to get a uniform response with the subsequent readout of a number of trailing pixels which is more than the physical number of pixels in the CCD in order to obtain overscan areas in both directions (vertical

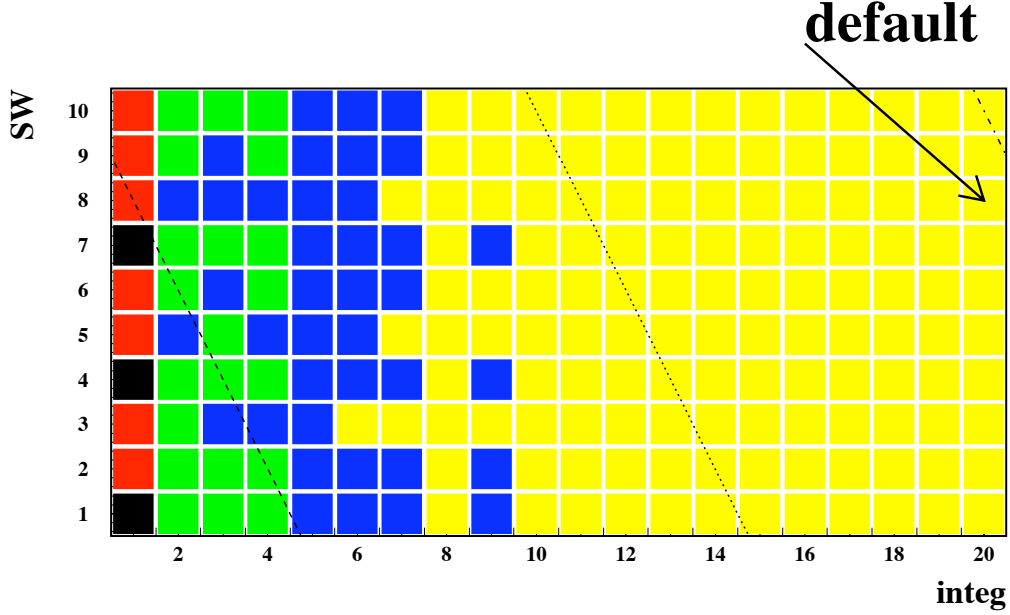


FIG. 5: Noise ( $\sigma$ ) in the DES CCD as a function of the width of the integration window (integ) and separation between the integration windows in the CDS (SW). The plot is made in steps of 50 nsec. Since the CDS uses two integration windows, an increase by a 50 nsec step in integ means an total increase in the pixel readout time of 100 nsec. The colors correspond to different noise levels: yellow  $\sigma < 10$  e, blue  $10 < \sigma < 15$  e, green  $15 < \sigma < 20$  e, red  $25 < \sigma < 30$  e and black  $\sigma > 30$  e. The diagonal lines correspond to fixed pixel times of  $4 \mu\text{s}$ ,  $5 \mu\text{s}$  and  $6 \mu\text{s}$ , from left to right respectively. The additional delays for the pixel readout (including the reset, horizontal transfer and digitization) and kept constant in this study, the pixel time is  $4.9 \mu\text{sec}$  for integ=10 and SW=8. The arrows point to our current default setting for these delays.

and horizontal). The amount of charge spilled out of the last physical column/row into the overscan, or equivalently, the amount of deferred charge, is measured with respect to the pedestal level.

An example of the data obtained in the transition between the readout of the physical pixels and the overscan is shown in Fig.7. The charge for the last physical pixel has to be shifted by 1024 pixels before it is readout. This method measures the charge deferred after the last physical pixel to estimate the inefficiency as  $\text{CTI} = \eta/1024$ , where  $\eta$  is the fraction of the charge of the last physical pixel that was deferred to the first overscan pixel.

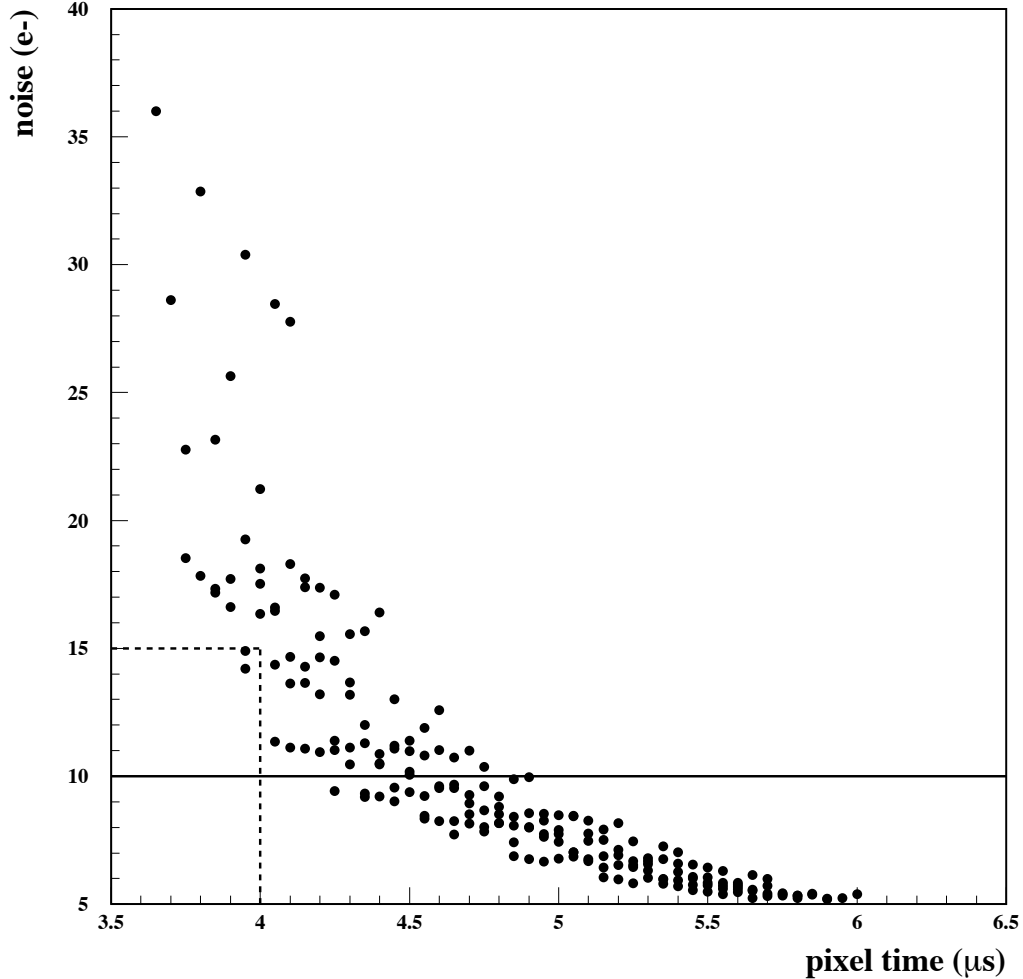


FIG. 6: Noise measurement as a function of readout time per pixel for the same points presented in Fig.5

Figure 8 shows the calculated CTI for the same device presented in Fig.7. The horizontal line indicates the DES technical requirement T-14 in Table I. The data shows that this detector satisfies the specifications for  $H+ > 6.5V$ .

The CTI on our CCDs has been measured using the EPER method for the horizontal and vertical directions. This is done for every new CCD that we test. Up to now we have been able to find a single set of operating voltages that makes every CCD meet the technical requirement T-14 (this is true for CCDs that are otherwise good devices). These voltages

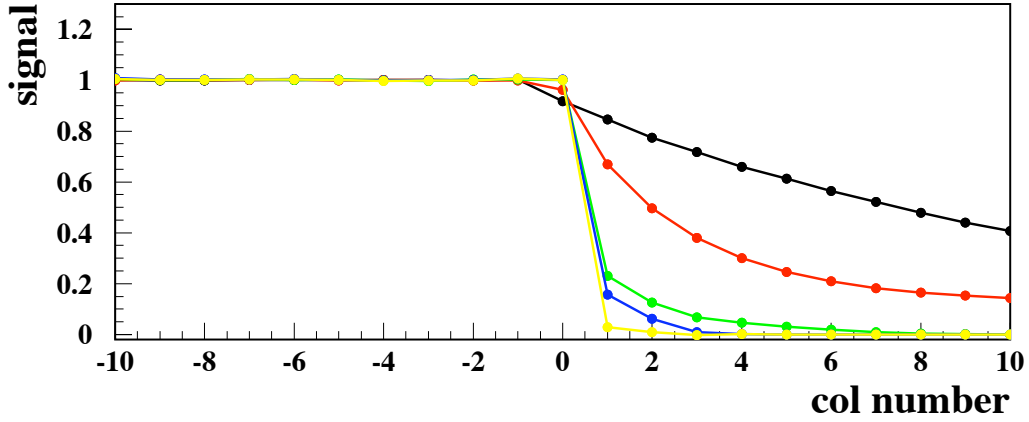


FIG. 7: Example of data used for the EPER analysis. The physical pixel are to the left of the image (negative column number) and the extended pixels or overscan is at the right (positive column numbers). In this case the transition to the horizontal overscan is shown. The pedestal is subtracted and the data normalized to the mean value in the physical pixels. The colors correspond to different positive rails of the horizontal clocks ( $H+= 4.0\text{ V}, 4.5\text{ V}, 5.0\text{ V}, 5.5\text{ V}$  and  $6.0\text{ V}$ ), with the highest voltage producing the sharpest transition.

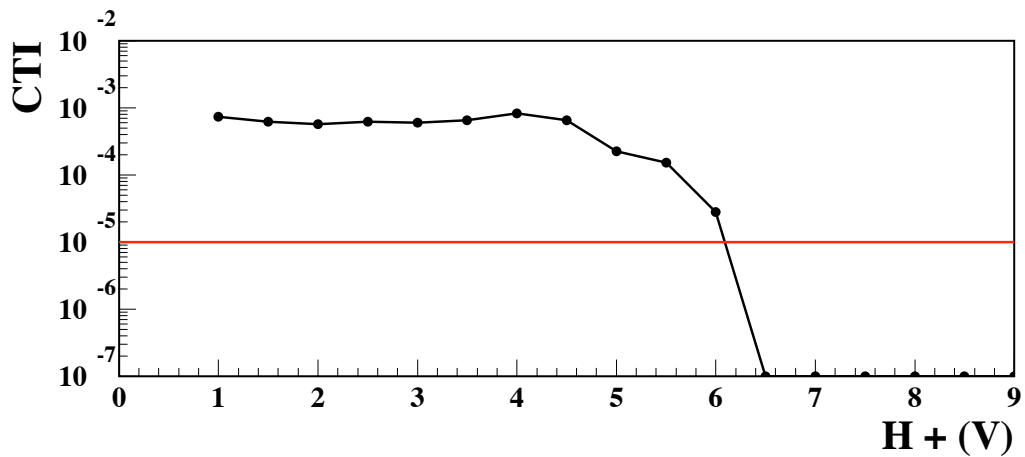


FIG. 8: Horizontal CTI calculated with the EPER method as a function of the positive rail of the horizontal clock ( $H+$ ). The horizontal line represented the DES technical requirement.

are shown in Table II (the table also shows the bias voltages used for this CCDs).

signal	voltage (V)	description
H+	8.5	positive rail horizontal clocks
H-	-4.5	negative rail horizontal clocks
V+	5.5	positive rail vertical clocks
V-	-2.5	negative rail vertical clocks
SW+	5.0	summing well positive rail
SW-	-5.0	summing well negative rail
TG-	-2.5	transfer gate negative rail
TG+	5.5	transfer gate positive rail
RG-	-6	reset gate negative rail
RG+	0	reset gate positive rail
$V_{OG}$	3.6	output transfer gate bias
VDD	-22.0	output drain voltage
$V_{REF}$	-12.5	reset drain voltage
$V_{SUB}$	40	substrate voltage

TABLE II: Clock voltages for DECam CCD operation. The bias voltages are also presented.

Another method for the measurement of the CTI is based on X-ray exposures. The idea is to expose the CCD to X-rays of 5.9 keV from Fe55, that will deposit 1620 e- into a single pixel (there are X-rays of other energies emitted from the Fe55, but the 5.9 KeV peak is the most prominent). For a device with perfect transfer efficiency, the measured charge will correspond to the deposited number of electrons. In the case of a significant CTI, the readout will give a different amount of charge depending on the position of the X-ray hit in the CCD.

This X-ray technique is based on the assumption that the energy deposited by an X-ray hit is restricted to 1 pixel. Because the DECam detectors are 250  $\mu\text{m}$  thick and back illuminated, charge diffusion makes the assumption of single pixel hits invalid (see discussion about charge diffusion below). However, these CCDs can be packaged as front illuminated detectors and exposed to X-rays from the front (this package will not be useful for the focal plane). We have packaged a few 250  $\mu\text{m}$  thick devices in this way, and here we present a

measurement of the CTI using X-rays in one such detector (PF-24-25). Figure 9 shows the X-ray spectrum measured for the detector (for a detail view of the X-ray peaks see Fig. 10). The horizontal CTI is calculated by measuring the position of the peak as a function of column number, as shown in Fig.11; this data can then be used to calculate the CTI as presented in Fig.12. The CTI measured for this CCD at the standard operating voltages using X-rays is consistent with  $CTI < 10^{-5}$  as required by T-14. We have done the same exercise for the vertical CTI, and the results are shown in Fig.13.

## VI. QUANTUM EFFICIENCY (T-20 ,T-21 AND T-23)

### A. Absolute QE (T-20)

The absolute quantum efficiency (QE) of the detectors is the only CCD technical requirement that is uncommon for a typical astronomical CCD. The science goals of our survey require high efficiency in the "z" band ( $> 65\%$ ). We define the absolute QE as the ratio of the number of electrons ( $\# e$ ) generated and captured per incident photon ( $\# \text{ photons}$ ) at a given wavelength for a given unit area.

$$QE(\lambda) = \frac{\#e}{\#\text{photons}} = (N_{ADU}/G) \frac{hc}{Pt\lambda} \quad (1)$$

where  $N_{ADU}$  is number of ADC counts measured,  $G$  is the overall gain (ADU/e-),  $h$  is Planck's constant,  $c$  is the speed of light,  $P$  is the incident optical power at the CCD surface,  $t$  is the exposure time and  $\lambda$  is the incident photon wavelength. An accurate measure of the absolute quantum efficiency is directly dependent on an accurate measure of the gain and the incident optical power at the CCD. The gain is determined by the photon transfer curve technique [5]. Our measurements give a gain uncertainty of  $\approx \pm 3\%$ .

Determination of the absolute optical power at the CCD is non trivial. For the absolute optical power measurement, we mounted a calibrated Hamamatsu photodiode in a picture frame package, very similar to that used for the DES CCDs. This detector was then mounted inside the dewar at the CCD location. We then measure the ratio of the incident optical power in the Hamamatsu photodiode relative to an Oriel calibrated photodiode mounted on our integrating sphere as a function of wavelength. Figure 14 shows the illumination configuration we use to measure this ratio of optical power. Without changing the optical setup, we replaced the Hamamatsu detector with the DECam CCD and measured the absolute optical

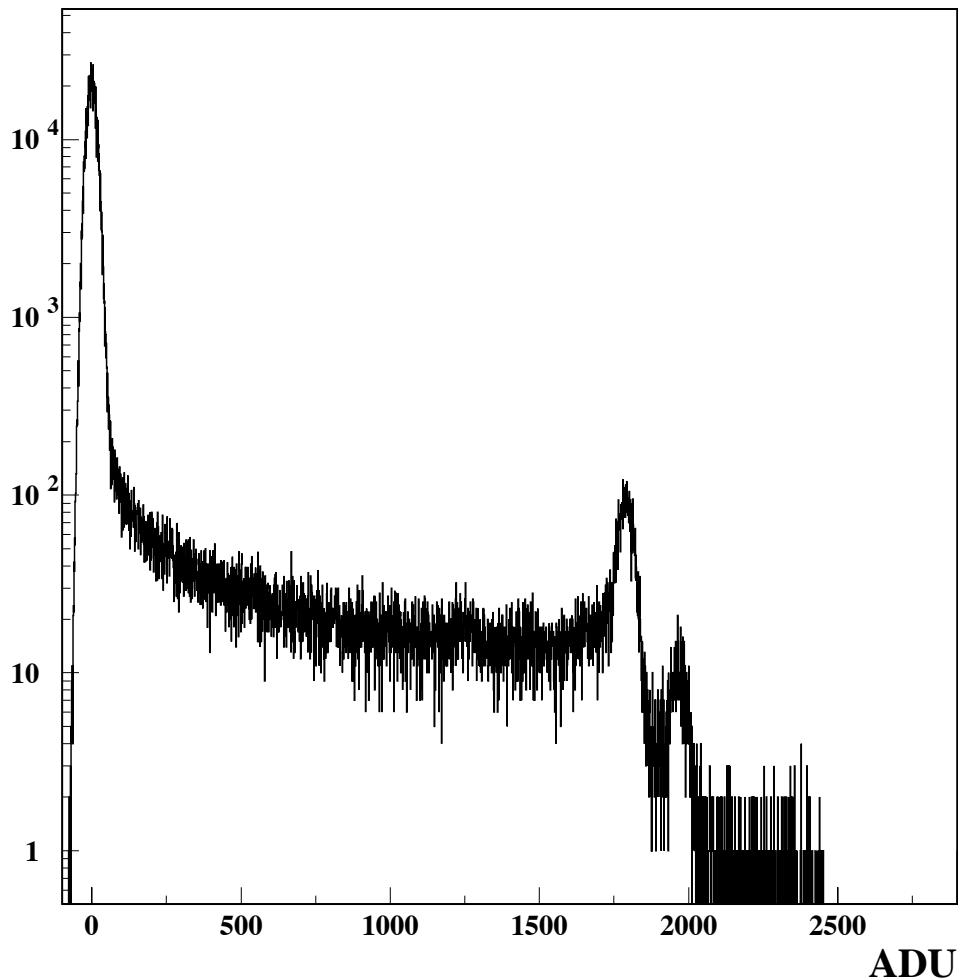


FIG. 9: X-ray spectrum measured for a front illuminated DECam CCD. The pedestal has been subtracted. The peak around 1700 ADU corresponds to the 1620e deposited in single pixel hits by the X-rays of 5.9 keV. A less significant peak corresponding to 6.5 keV is also seen.

power at the CCD at different wavelengths. Figure 14 shows our setup. Two integrating spheres are necessary to eliminate unwanted structure light effects from the source lamp at either the Oriel calibrated photodiode or the output port to the CCD. These structured light effects introduce uncertainties in measurements of the incident optical power at the CCD.

Figure 14 also shows the illumination configuration we use to measure a CCD’s absolute quantum efficiency. Measurements of the absolute quantum efficiency for a single device are

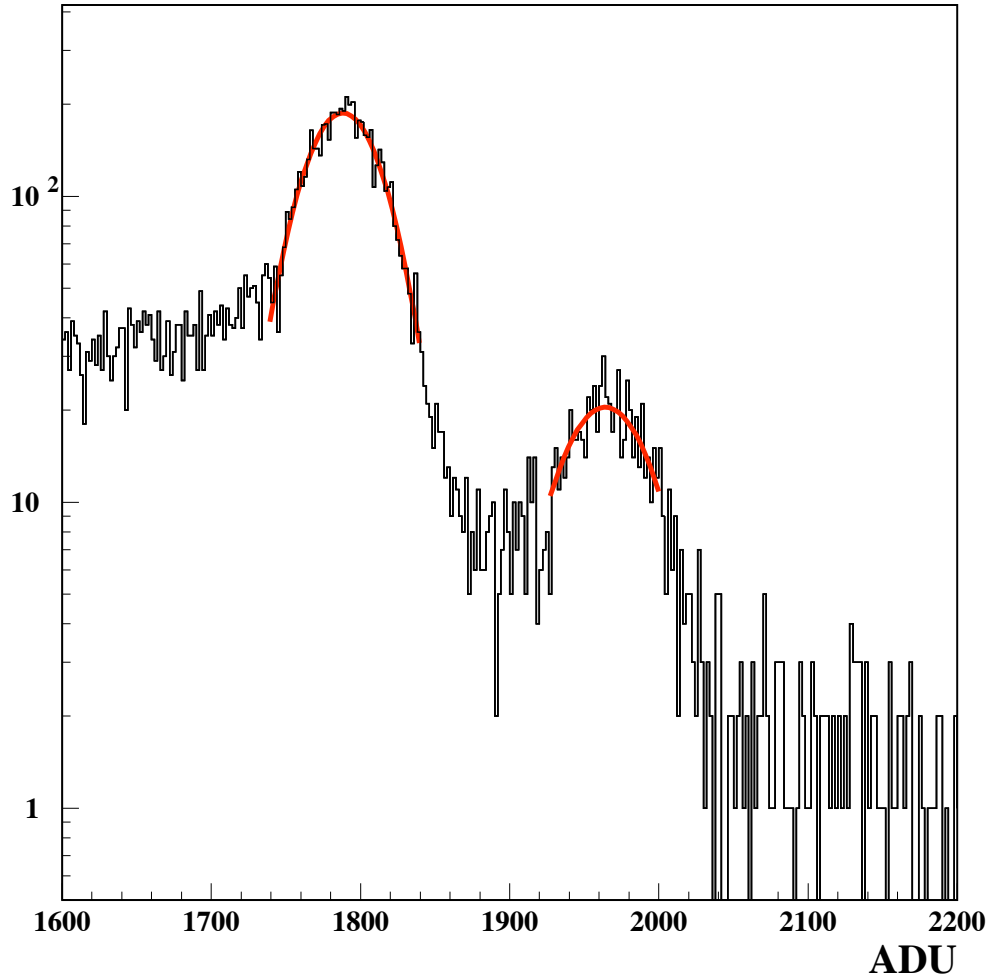


FIG. 10: Detail of Fig. 9. The peak at 1788 ADU corresponds to the  $K_{\alpha}$  X-ray with 5.9 keV, depositing 1620e . The peak at 1964 ADU corresponds to the  $K_{\beta}$  X-ray with 6.5 keV, depositing 1778e.

shown in Fig. 15. The figure shows the absolute QE for both the right and left readout channels. Data for a different CCD measured at LBNL is also shown for comparison.

Some of the technical requirements on the QE of a CCD can be determined by measuring the relative QE of a device. The relative QE is defined as the ratio of the QE at a given wavelength to the QE of the same device at a fixed wavelength. Relative QE removes the uncertainty of gain and the sphere-to-dewar ratio of optical power. Fig. 16 gives the relative

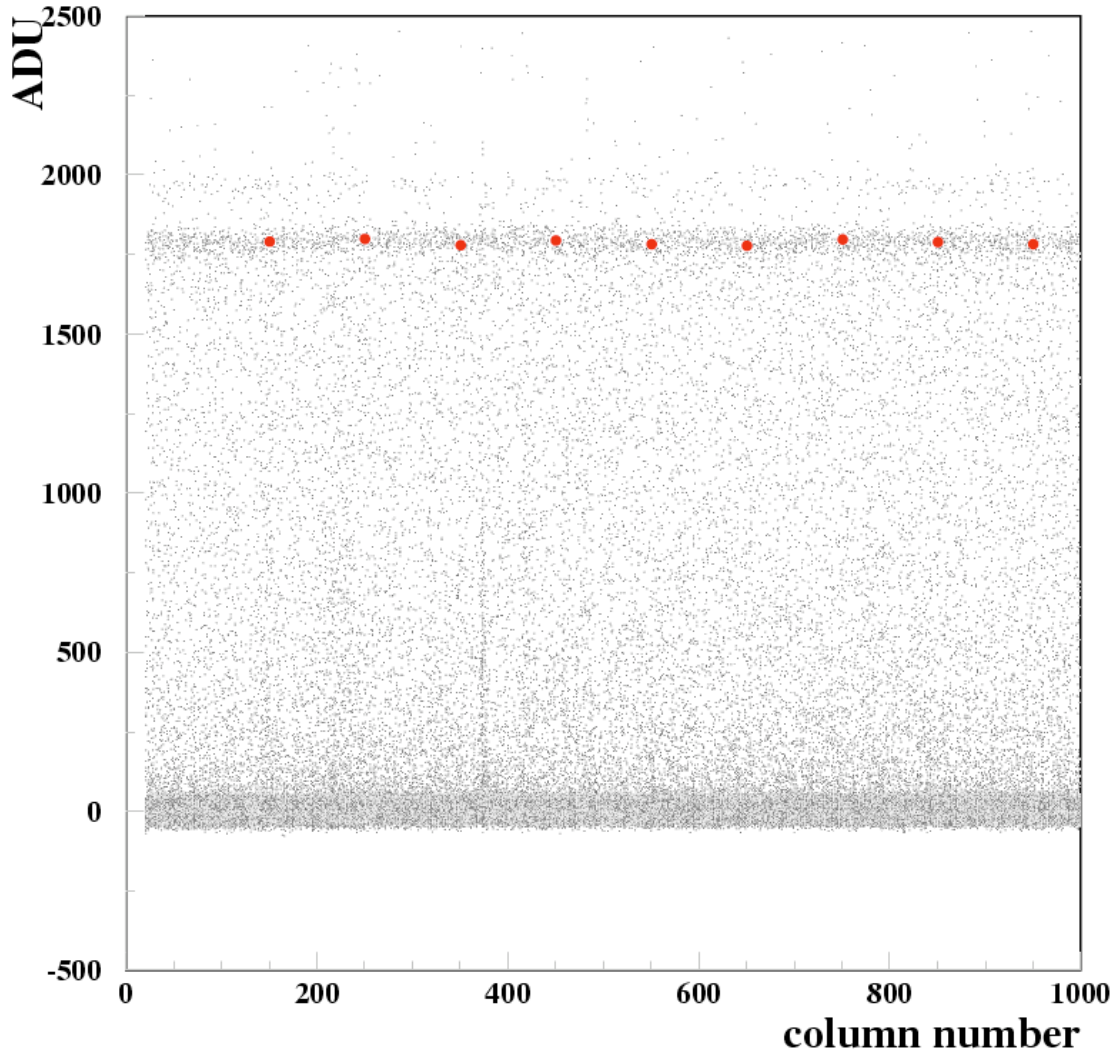


FIG. 11: ADU shown in the Y-axis as a function of column number (X-axis). The peak from the 5.9 keV X-ray is evident as a region of higher concentrations of points around 1778 ADU. The red circles measure the position of this peak as a function of column number.

QE for two engineering CCDs relative to 800 nm.

### B. QE stability (T-21)

In addition to the technical requirement on the absolute QE, the DECcam project also has requirements on the stability of the QE. Of particular interest here is the QE dependence on temperature. The QE for the red part of the spectrum is expected to be the most sensitive to temperature changes in the focal plane. Using a monochromator we study the relative

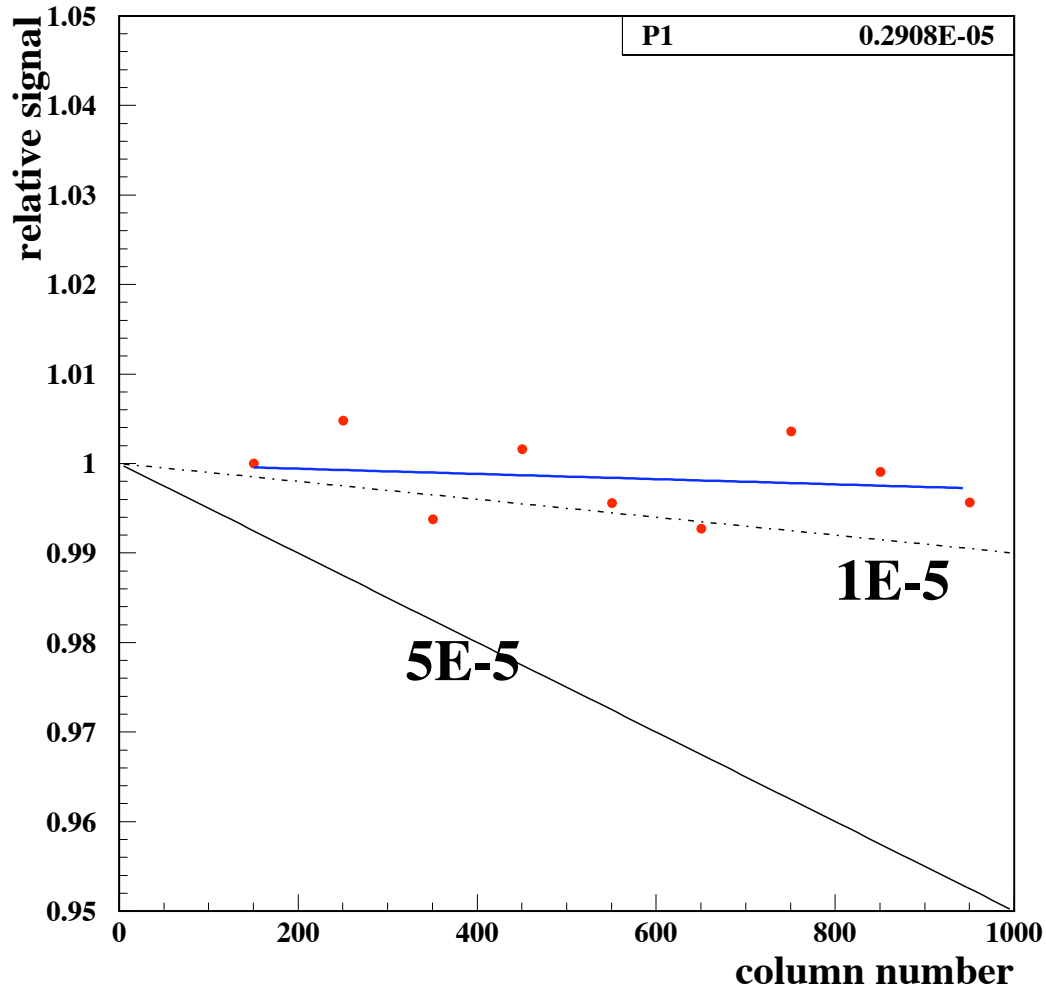


FIG. 12: Horizontal CTI measurement using Fe55. Fraction of charge measured for the 5.9 keV X-ray peak (see Fig.11) as a function of column number. A significant horizontal CTI will correspond to a slope in this plot. Example lines are shown for  $CTI=1E-5$  and  $5E-5$  (black lines). The data is consistent with  $CTI=3E-6$  (fitted blue line).

QE as a function of temperature for the longer wavelength part of our sensitivity range. The results are shown in Fig. 17 and Fig. 18. The plots show a 5% QE change at 1000 nm when the temperature changes by 10 K and a 1% QE change for a 5 K temperature change (in this case we have included data for 2 CCDs because, in the following section the device-to-device differences are considered). This indicates that to achieve technical requirement T-21 we

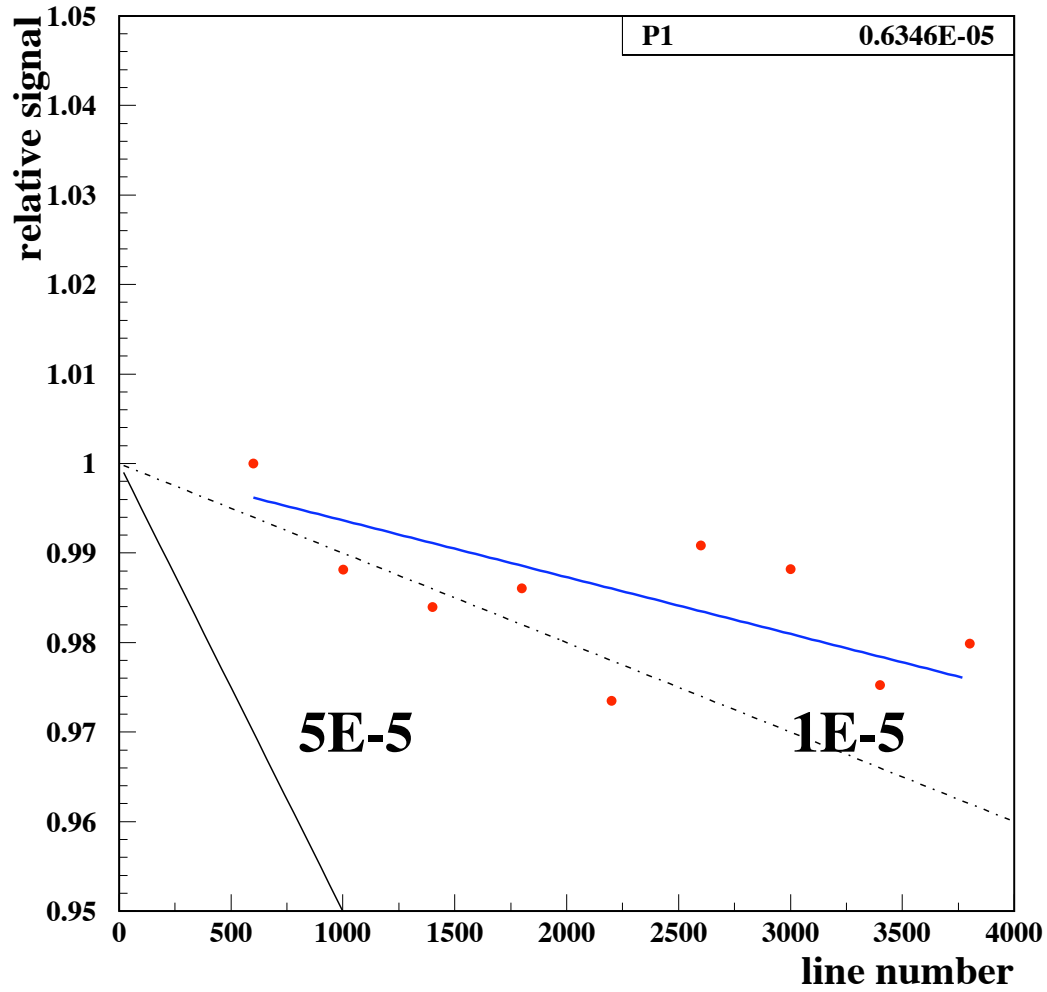


FIG. 13: Vertical CTI measurement using Fe55. Fraction of charge measured for the 5.9 keV X-ray peak (see Fig.11) as a function of line number. A significant vertical CTI will correspond to a slope in this plot. Example lines are shown for CTI=1E-5 and 5E-5 (black lines). The data is consistent with CTI=6E-6 (fitted blue line).

need a temperature stability of the focal plane of 1 K.

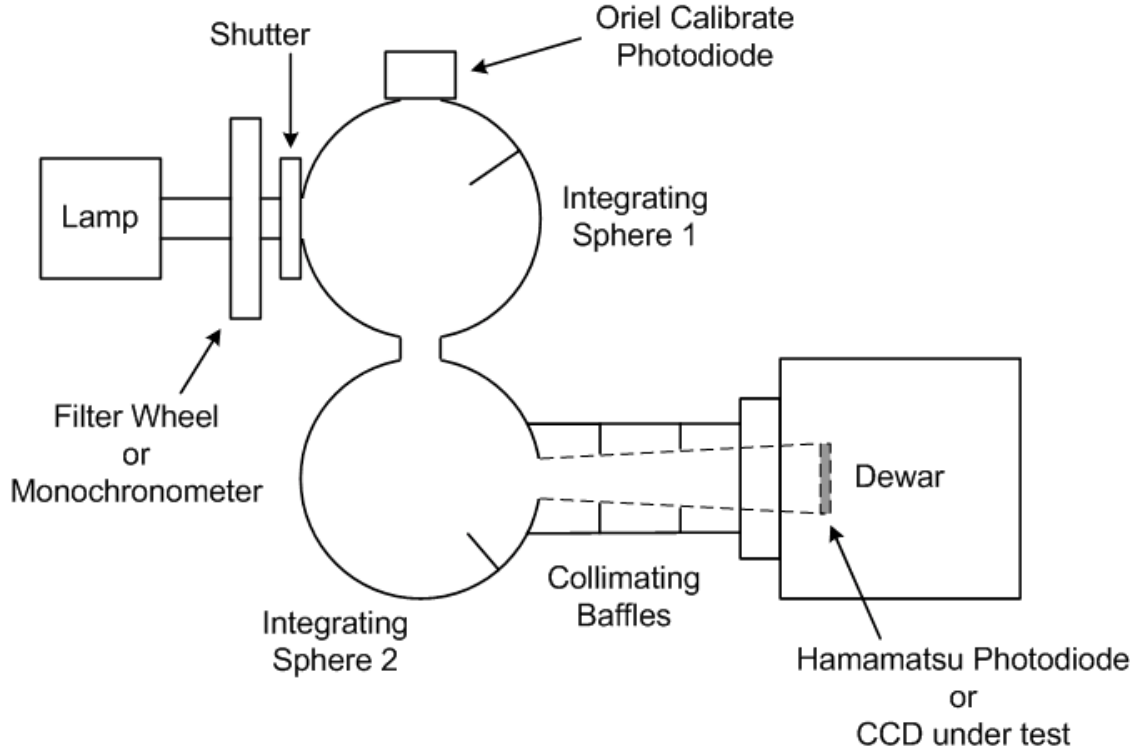


FIG. 14: Illumination setup for absolute QE measurements. The this figure shows the method used to either (1) determine the ratio of optical power at the CCD relative to the optical power in our integrating sphere or (2) measure a CCD absolute QE.

### C. QE uniformity (T-23)

The technical requirement T-23 states that the absolute QE of the detectors in the focal plane has to be uniform to 5%. The current plan does not include a selection of the CCDs to accommodate a temperature gradient on the focal plane to achieve this requirement. Considering the results presented in Fig. 17 and Fig. 18, this requirement means that the temperature of the focal plane has to be uniform to 10 K.

T-23 also imposes a requirement on the QE differences between devices. Extensive studies on this aspect of T-23 have not been done (QE measurements need to be performed on a larger sample of detectors). Figure 16 shows better than 5% consistency in the relative QE between the two CCDs. The measurements at wavelengths below 500 nm show the largest difference and more detectors need to be studied to understand if this difference could be due to a non-uniformity in the antireflection coating between the 2 CCDs.

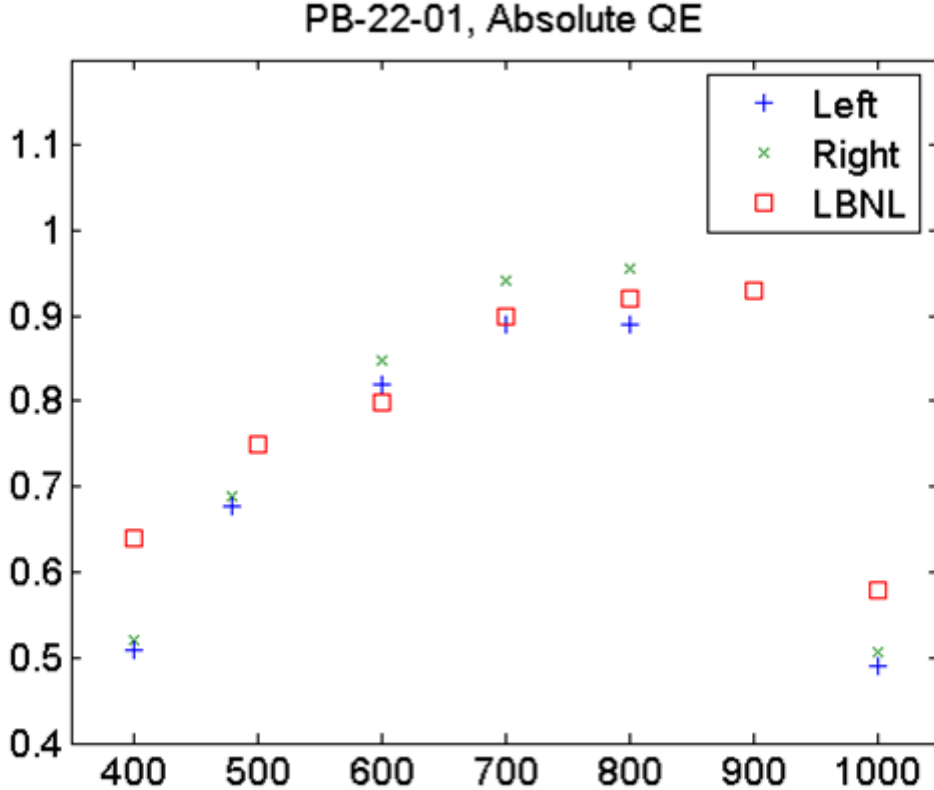


FIG. 15: Absolute QE for CCD pb-22-01 for both right and left readout channels. Data for a different CCD measured at LBNL is also shown for comparison.

## VII. CHARGE DIFFUSION (T-27)

We have developed a new technique for measuring the charge diffusion in a CCD and the details are discussed in Ref. [13]. Our method is based on imaging a diffraction pattern produced by a double slit (for a general description of optical diffraction see Ref. [6]); as a first step we describe this method using a simulation.

A typical example of a region of this diffraction pattern is shown in Fig.19. As can be seen in the image, there is a high and low spatial frequency component. The high spatial frequency component corresponds to a spatial period of approximately 5 pixels.

In previous work [3] [8] it has been shown that for these CCDs the spatial variance resulting from diffusion ( $\sigma_d^2$ ) depends on the substrate voltage ( $V_{sub}$ ) used to achieve depletion. For example if  $V_{sub}$  is reduced, allowing extra diffusion in the CCD, the image smears, making the high spatial frequency component weaker, as shown in Fig. 20. By measuring

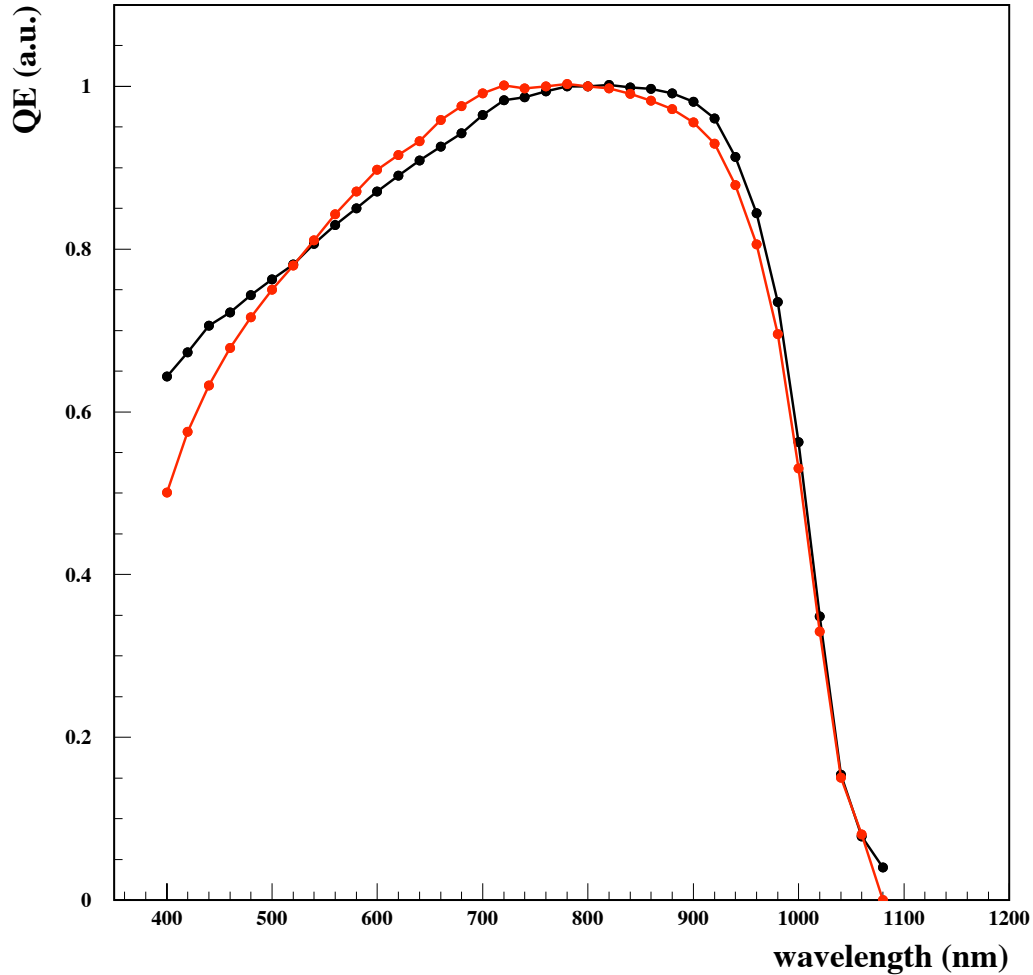


FIG. 16: Relative QE (normalized at 800nm) compared for two DECCam CCDs from engineering productions runs Lot 1A (red) and Lot 1B (black).

the difference in the Fourier power spectrum between Fig.19 and Fig.20, one can quantify the increase in diffusion produced by the reduction in  $V_{sub}$ . More details are presented in Ref.[13].

The results for diffusion measurements in our detectors are presented in Fig.21. They correspond to three 2k x 2k CCDs from DECCam engineering runs and are compared with results published in previous work [8] obtained for a SNAP[7] CCD. The DECCam CCDs have been certified to support up to  $V_{sub} = 40$  V. The long term performance of the devices could

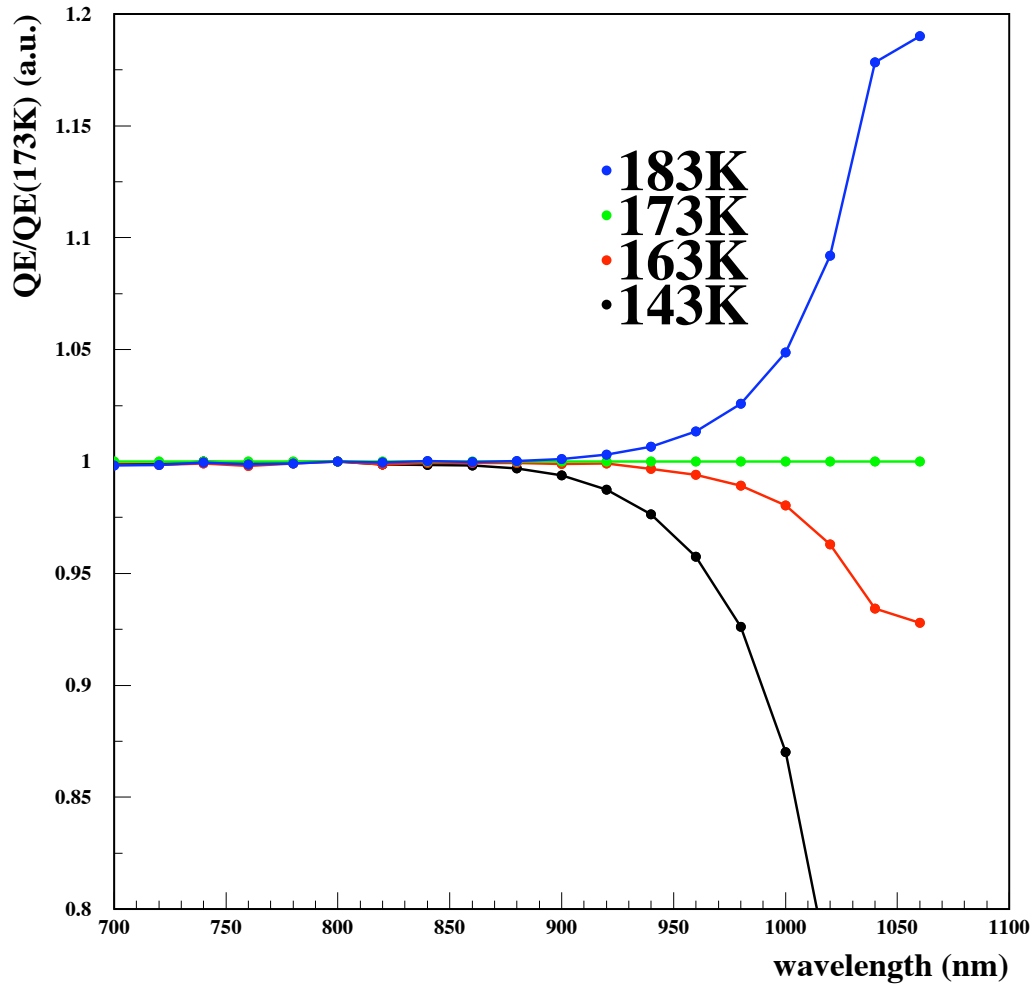


FIG. 17: QE relative to that measured at the operating temperature (173K) as a function of wavelength.

be compromised at higher voltages. The tests done for this work included measurements with  $V_{sub} > 40V$ , but these higher voltages were applied to the device only for a short time (a few minutes). The results obtained indicate that for  $V_{sub} = 40 V$  the tested DES CCDs have a dispersion due to charge diffusion of  $\sigma_d < 7.5 \mu m$ , as established in the technical requirement T-27. Table III shows a comparison of the results of this work with previous studies. The table also shows the diffusion obtained with “spot-machine” for a higher substrate voltage SNAP device [8].

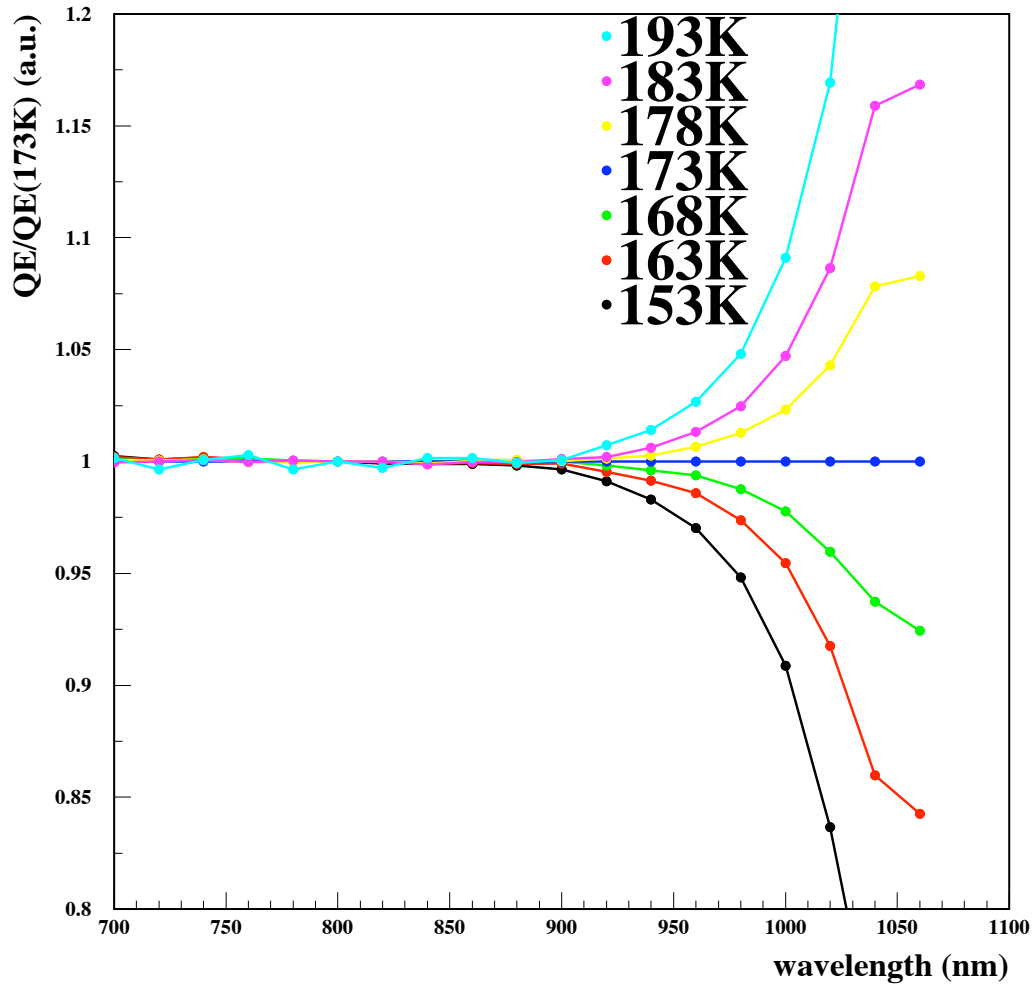


FIG. 18: QE relative to that measured at the operating temperature (173K) as a function of wavelength, for pb-22-04.

The technique used here simplifies significantly the setup needed for the measurement with respect to the more traditional “spot machine” method and will permit the characterization of the diffusion in a large number of the DECam CCDs. However, the new technique is not capable of making a localized measurement of diffusion in a very small area of the sensor. This measurement can be done with the more sophisticated setup corresponding to the “spot machine”. We expect to measure diffusion for some of our detectors in the detector testing laboratory at University of Michigan, for these DES collaborators have a

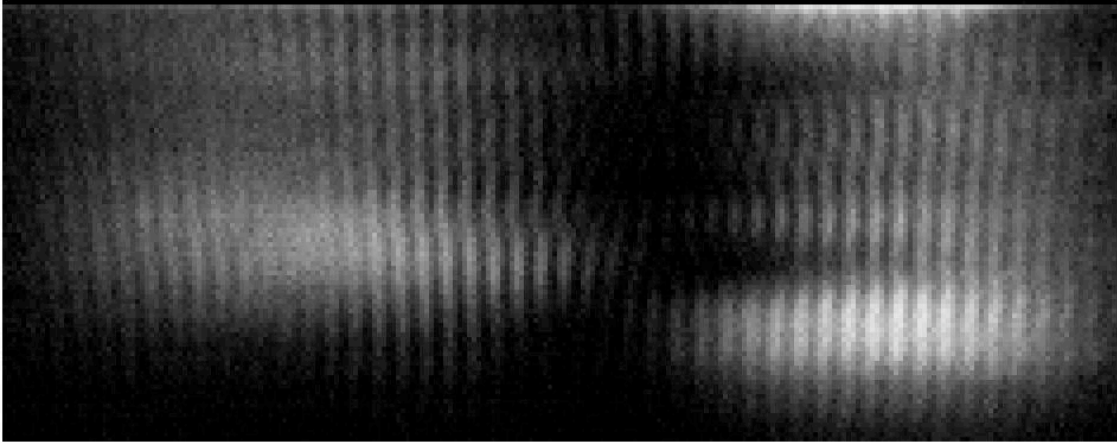


FIG. 19: Double slit diffraction pattern produced with two slits of width  $100\ \mu\text{m}$ , separated by  $1\ \text{mm}$ , illuminated with a laser, and imaged with a  $2\text{k} \times 2\text{k}$  CCD  $200\text{mm}$  away from the slits. The CCD is a back illuminated,  $250\ \mu\text{m}$  thick device from the engineering run of DECam CCDs. For this image the CCD was operated with  $V_{sub} = 70\text{V}$ . The image shows only a small fraction of the full pattern, corresponding to the region used for the analysis described below.

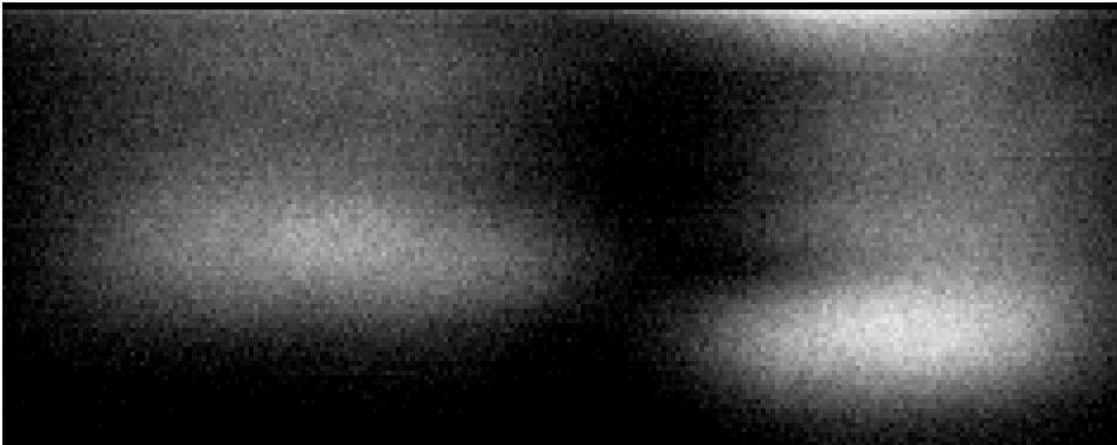


FIG. 20: Same as Fig. 19, but now reducing the substrate voltage to  $V_{sub} = 10\ \text{V}$ .

spot machine.

### VIII. FLATNESS (T-28 AND T-29)

The CCDs for DECam are packaged on a pedestal module that gets mounted to the focal plane. The science package for our detectors is shown in Fig. 22. A detailed description this

CCD	$\sigma_d$ ( $\mu\text{m}$ )	thickness ( $\mu\text{m}$ )	method	$\sigma^2(70\text{V})$ ( $\mu\text{m}^2$ )	$\alpha$ ( $\mu\text{m}^2/\text{V}$ )	$\tilde{\sigma}^2(70\text{V})$ ( $\mu\text{m}^2$ )
pb-22-01	$6.1 \pm 1.2$	250 (DECam)	double slit	$24.9 \pm 4.8$	$1491 \pm 253$	$25.0 \pm 5.4$
pb-22-03	$7.2 \pm 0.8$	250 (DECam)	double slit	$37.3 \pm 4.5$	$2197 \pm 249$	$37.5 \pm 8.1$
pb-22-04	$5.8 \pm 1.0$	250 (DECam)	double slit	$22.0 \pm 7.0$	$1359 \pm 394$	$22.2 \pm 4.5$
Fairfield06 [8]	$3.7 \pm 0.2$	200 (SNAP)	“spot machine”			
Rodney06-A [10]	1.5	20	X-ray			
Rodney06-B [10]	4.6	45	X-ray			

TABLE III: Diffusion measurements for the three CCDs studied in this work compared with previous results. All the CCDs in the table have 15  $\mu\text{m}$  pixels, except for the Fairfield06 device with 10.5  $\mu\text{m}$  pixels. The measurements correspond to  $V_{sub} = 40$  V for the first three devices in the table,  $V_{sub} = 115$  V for Fairfield06 and no substrate voltage applied for Rodney06-A and Rodney06-B. The error in our measurement is estimated by looking at different regions of the CCD with the same diffraction pattern.

package is presented in Ref. [14]. Finite Element Analysis has been done to understand the thermal distortions of the imaging surface of the detector in the package (this will contribute to the flatness of the cold package). These studies are discussed in Ref. [15]. An example of the results is presented in Fig. 23 showing a maximum thermal distortion of 5.2 microns  $\mu\text{m}$ .

A flatness scanning system has been developed at FNAL using a confocal chromatic displacement measurement system from Micro-Epsilon Corp. This device takes light from a halogen bulb and directs it such that light of different frequencies is focused at different distances from the instrument head. The wavelength of the light reflected back from the focus spot is sensed by the system and is an indicator of the illuminated surfaces distance from the instrument head. The advertised accuracy of this device is approximately 0.05% linearity over a 24 mm range with a maximum working distance of almost 250 mm. The positioning system used to guide the scanning head must have exceptional straightness in order to utilize the accuracy of the instrument, for variations in stage straightness will directly impact measurement accuracy. A set of motorized stages from Physik Instrumente with a straightness of 1 micron per 100 mm of travel was therefore selected. The 300 x 300 mm travel range of the system is not large enough to measure the entire surface of the

completed camera array, but it will allow coverage of a significant portion of it such that the flatness of the entire array can be mapped from a small number of overlapping measurement fields. The scanning system is shown in Fig. 24.

The scanner and translation stages are controlled with a LabView program designed to survey a grid of points on the CCD surface. The grid spacing is an input parameter and we typically use a 500 micron step. Each data point is actually the average of 20 consecutive readings taken at that position, and the standard deviation of the measurements is typically 4 microns. A full scan of the surface, with about 7800 grid points, takes about 90 minutes. The flatness analysis is done averaging the results of two full scans.

Due to the mechanical requirements for this test, the detectors need to be installed in a dewar dedicated to this task, which introduces additional detector handling steps. This test has been done on most non-functional science packages of the type described in Ref. [14] and shown in Fig. 22. An example of the results obtained is presented on Fig. 25. The analysis of the data presented here shows  $< 3 \mu\text{m}$  deviation from flat in square regions of 1 cm x 1 cm (this corresponds to the r.m.s. of the measurements done in the square region) indicating that the CCD satisfies the technical requirement T-28. None of these 1 cm x 1 cm regions show deviations to a neighboring region of more than  $10 \mu\text{m}$ , thus the package meets the technical requirement T-29. All four packages tested have passed the flatness specifications.

## **IX. COSMETIC DEFECTS (T-30)**

The cosmetic defects are studied by detecting the pixels that are 5% above or below background level in a flat field image. To eliminate the cosmic rays from the analysis, a sequence of 10 images was taken with a fixed illumination level. Dark exposures were taken along with the flat fields and subtracted before the analysis was done. The median image was produced using the 10 flat fields.

Here we present the cosmetic defects studies done for a picture frame back illuminated, 2k x 2k CCD (pb-22-04) from engineering Lot 1B. We have been reserving our best 2k x 4k devices for packaging in the final science module, which we are still developing. We expect that the 2k x 2k devices (like pb-22-04) are a good approximation to the defects that we will encounter on the untested 2k x 4k. The picture frame packages have edge features that

are not expected on the science modules, so we have eliminated the edges of the imaging area from the analysis (14 columns were removed on the sides of the CCD, 300 rows at the bottom and 150 at the top).

The median image is shown in Fig. 26. An object detection algorithm was used to identify pixels that deviated from the background level by more than 5% [16]. The detected objects are shown in Fig. 27. Table IV summarizes the number of detected defects categorized by defect size location (left or right). The table shows the the pixels above (+5 %) and below (-5 %) background. The total fraction of the pixels affected was 0.78%.

Technical requirement T-30 establishes an average of 5% unusable area for the CCDs mounted on the focal plane (this is in addition to the 10% non imaging area of the focal plane introduced by mechanical design). After considering the the edges (1.5%) and the possibility of losing one detector (1.6%), we have a budget for non usable pixels of 1.9 %. The number of pixels affected by cosmetics for the CCD analyzed here is below budget. In Ref [4] a conservative approximation is suggested to account for the PSF size while considering the effect of a completely bad column (each bad column is taken as producing a 5 column unusable area due to the PSF size of 2 pixels). This approximation has not been extended to defects of more general shapes considered in this analysis.

## Traps

Charge traps in CCDs are localized defects that trap electrons from subsequent pixels in a column during readout, and can affect CTE. Typically modern CCDs have a low level of traps present in new devices, but traps can be created due to radiation damage. DES is not expected to have problems with radiation damage, so the emphasis for us is to monitor device quality, quantify the effect of traps on CTE, and look for traps large enough or clustered in a small enough area to affect science performance.

The best way to look for traps is to use pocket pumping (for details see Ref. [5]), which means before a certain row is read out, the vertical clock is reversed for multiple pixels (in our case ten pixels) and then cycled forward and back thousands of times. This is meant to drain most of the charge from the ten pixels and trap it in the one pixel with the trap. The DES CCD testing team has implemented pocket pumping and can choose the number of reversed clocks and number of cycles with the input GUI in an automated fashion.

In order to increase the number of traps and optimize our trap algorithms, a 512 x 1024 pixel CCD (device pb-512-15) was irradiated in the FNAL neutron therapy medical facility. Figure 28 shows a 2-D plot of row number versus column number, color keyed by the median ADU (over 5 exposures) in each pixel. The black vertical areas that are ten pixels tall have a hot pixel adjacent to them that has collected all the charge, and are textbook traps. We have also observed traps in devices that have not been irradiated, Fig. 29 shows one example: one column from a 2kx2k CCD (pb-22-04) with an obvious trap. With a very loose definition of traps, we found about 10 times more traps in the irradiated device.

We have taken trap data with different numbers of reversed clocks, cycles, and light levels. The behavior is as expected. However, in addition to the textbook traps presented in previous figures, we have observed many variations of trap-like objects in the pumping data, that do not appear without pumping. We are currently studying these variations. We have also taken data with different temperatures which is under study.

The study of traps in DECam detector is in its early stages, but we have clearly observed them with pocket pumping and are continuing to study them under different conditions. The number of traps in our CCDs will contribute to the number of defects related to the technical requirement T-30.

## **X. DARK CURRENT (TP-1)**

The dark current specification for the DECam detectors is 25 e/pix/hour. The measurements of dark current for our example detector are shown in Fig. 30. The results indicate that the technical specification for DECam is achieved below 180 K. In order to select an operating temperature for the CCDs, we also studied the QE as a function of temperature, as shown in Fig.31.

Since the QE for wavelengths around 1000 nm drops significantly when the temperature is reduced, we take 173 K as our operating point. The quality of our production CCDs will tell us if we can stay with this selection or if we have to operate colder to keep the dark current low. At 173 K the detector meets the preliminary technical specification TP-1.

## XI. CROSSTALK (TP-2)

A detailed study of the CCD and front end electronics crosstalk is discussed in Ref. [11]. Only the main results of that work are discussed in this document. The crosstalk between the neighboring channels in the front end electronics (FE) is shown in Fig.32. The measured crosstalk is  $X_{FE} = 8 \times 10^{-4}$  (for the non-neighboring channels the crosstalk in the FE is at least a factor of 10 smaller).

The crosstalk between the two CCD channels was measured using the FE channels which present the lowest crosstalk ( $< 4 \times 10^{-5}$ ). The measured crosstalk between the two CCD channels is  $X_{CCD} = 7 \times 10^{-4}$ , shown in Fig. 33. These crosstalk measurements include the contribution from CCD packaging and cables inside the dewar.

The results show that  $X_{FE}$  and  $X_{CCD}$  satisfy the preliminary technical requirement TP-2 which specifies  $X < 10^{-3}$ . However, additional work needs to be done to achieve TP-2 for a CCD with its two outputs connected to neighboring channels in the electronics. This work will be done with the new 12-channel Monsoon acquisition board developed for DECam.

## XII. PLAN FOR PRODUCTION CCD TESTING

In this section we discuss our current plan for CCD testing during production. At the peak of the production rate we expect to test 5 CCDs per week. We estimate the need for 5 complete testing stations (we currently have three). We plan to have each new device go through a sequence of tests that will take up to 1 week for a good CCD.

### Stage 1 testing

Every packaged device will go through this step. At our peak production rate we expect to have 5 new packages per week. Stage 1 will usually run overnight and the data will be used to produce an automated report that should be ready about 1/2 day after data collection. Because part of our team is in Barcelona, we will benefit from the time difference.

#### 1. Photon Transfer curve

The photon transfer curve technique is described in detail in Ref. [5]. A set of images is taken with increasing light level, with two images at each light level. Assuming

Poisson statistics for the number of electrons per pixel, the gain can be obtained.

A photon transfer curve is produced for each CCD to confirm that the device satisfies technical requirements T-10, T-11, T12 and T-13.

The illumination level is fixed to produce 16000e for a 10 sec exposure. The exposure time is then varied between 10 sec and 100 sec (achieving a maximum signal of 160000e). The exposure times are first ramped up in steps of 10 seconds and then ramped down with similar steps, with an offset of 5 seconds. This will allow the distinction between a possible time dependence and a signal level dependence in the test. Twenty exposure times are used, with 2 images for each exposure time. A total of 40 images are produced.

## 2. Clock Rail Scan

Each of the four clock rails (horizontal upper and lower rail, vertical upper and lower rail) used for the charge transfer between pixels is varied between 0.5 V and 10 V in steps of 0.5 V. A 10 second exposure is taken for each voltage level. This corresponds to 20 exposures per clock rail with a total of 160 exposures.

The clock rail scan is performed to verify the technical requirement on charge transfer inefficiency (CTI) T-14. Since we have found a set of clock levels that work for every tested CCD passing T-14, this step is not strictly needed. However, we decided to proceed in this way in order to verify the CTI and noise dependence on the clock level for each CCD. This step also allows us to understand the possible dependence of any defect on the clock levels.

## 3. Output Gate Transfer

Also part of our full characterization for each CCD is the measurement of the output transfer gate curve, as described in Ref. [5]. The goal is to measure the voltage at which charge injection is produced in the device as a function of  $V_{REF}$  (reset drain voltage). This technique allows the determination of the channel potential inside the CCD, under the output gate. Charge injection occurs when this voltage is lower than  $V_{REF}$ . The difference between the applied gate voltage and the channel voltage is typically called  $V_{th}$  and depends on the doping conditions of the silicon. This test is not strictly necessary and does not address any specific technical requirement. These

measurements allow us to confirm that the operating bias voltages chosen make sense and to learn how the performance of the detectors changes when the bias voltages move. A total of 162 images are taken for this test.

#### 4. Charge Pumping

Charge pumping studies will be done for each device with the objective of detecting low level traps in our detector which will contribute to the technical requirement T-30.

The number of pumped lines will be varied as well as the illumination levels. Several exposures are taken in each condition to eliminate cosmic rays and to increase the significance for the detection of traps. This will correspond to approximately 64 exposures (including darks for each configuration).

#### 5. Sets of 10 dark and flat exposures with two different exposure times

This data will be collected for cosmetic defects detection for the verification of technical requirement T-30. A total of 40 exposures will be produced.

### **Stage 2 testing**

Devices passing Stage 1 testing will remain cold for further studies. This additional tests will take approximately 2 more days.

#### 6. Quantum Efficiency Measurements

The QE measurement will be done using a 6 position filter wheel and will measure the absolute QE with a precision of 10% for the narrow band filters 400, 500, 600, 800, 900, 1000 nm. A set of dark and flat exposures is taken for each filter position, producing a total of 12 exposures. This step is done to verify T-20.

#### 7. Charge diffusion Measurement

The current plan includes a charge diffusion measurement for each CCD that passes all other tests. This measurement is done to certify the technical requirement T-27.

The measurement will be done using the diffraction pattern as discussed above. We will measure the diffusion as a function of substrate voltage ( $V_{SUB}$ ) between 10 and 70 volts in 13 steps. This will correspond to 26 images.

## 8. Temperature Scans

Once all the other tests are performed on the CCD, we will measure the QE at 1000nm and the dark current levels as a function of temperature. For this we will turn off the temperature control of the system and shut down the LN2 supply. The CCD will then cool down ( typically will reach 120 K) and later warm up to room temperature in approximately 10 hours. During this time we will continuously take a series of 400 sec dark exposures followed by 10 sec darks and 10 sec flats (at 1000 nm wavelength). This will produce data as presented above for QE and dark counts as a function of temperature. This data will be used to certify T-21, T-23 and TP1. This will amount to approximately 200 exposures.

### **Stage 3 testing**

Device is removed from CCD testing station after 4 days. The CCD could then be moved to a flatness measurement station.

## 9. Flatness measurement

If needed, we could do a measurement of flatness on each CCD. In order to understand the need for this test, we have to accumulate more data on flatness for our prototype science packages. So far, all CCDs tested (4) pass the flatness requirements T-28 and T-29.

- 
- [1] Dark Energy Survey Collaboration, astro-ph/0510346.
  - [2] Flaugher, B., Ground-based and Airborne Instrumentation for Astronomy. Edited by McLean, Ian S.; Iye, Masanori. Proceedings of the SPIE, Volume 6269, (2006).
  - [3] S.E. Holland, D.E. Groom, N.P. Palaio, R. J. Stover, and M. Wei, IEEE Trans. Electron Dev. 50 (3), 225–238 (January 2003) LBNL-49992.
  - [4] T. Abbott, J. Annis, B. Flaugher, S. Kent, H. Lin and W. Merritt, "Science-Technical-Requirements", DES Document 20-v15.
  - [5] J.R. Janesick, Scientific Charge Cupled Devices, SPIE press (2001).

- [6] F.S.Crawford, McGraw-Hill, 1968.
- [7] “Supernova / Acceleration Probe: A Satellite Experiment to Study the Nature of the Dark Energy”, SNAP Collaboration, G. Aldering *et al.*, submitted to Publ. Astr. Soc. Pac., astro-ph/0405232; SNAP Collaboration, astro-ph/0507459.
- [8] Jessamyn A. Fairfield, D. E. Groom, S. J. Bailey, C. J. Bebek, S. E. Holland, A. Karcher, W. F. Kolbe, W. Lorenzon, & N. A. Roe, submitted to IEEE Trans. Nucl. Sci., (April 2006).
- [9] A. Karcher, C.J. Bebek, W. F. Kolbe, D. Maurath, V. Prasad, M. Uslenghi, M. Wagner, IEEE Trans. Nucl. Sci. 51 (5), (2004) LBNL-55685.
- [10] S.A. Rodney & J.L. Tonry, astro-ph/0604322.
- [11] J. Estrada and A. Plazas, ”Xtalk Measurements for DES CCDs and Monsoon boards”, DES Document 207-v1.
- [12] For more information on the Monsoon electronics see:  
[http://www.noao.edu/ets/new\\_monsoon/](http://www.noao.edu/ets/new_monsoon/)
- [13] H. Cease, H.T. Diehl, J. Estrada, B. Flaughner and V. Scarpine, ”Measurements of Charge Diffusion in Deep-Depletion CCDs by Optical Diffraction”, DES Document 371-v1.
- [14] G. Derylo, H. T. Diehl and J. Estrada, ”0.25mm-Thick CCD Packaging for the Dark Energy Survey Camera Array” , SPIE 2006, DES Document 59-v2.
- [15] G. Derylo, ”Updated FEA Study of 2kx4k Module V1 Design” , DES Document 173-v1.
- [16] We use ”SExtractor” by E. Bertin, for more detail:  
<http://terapix.iap.fr>

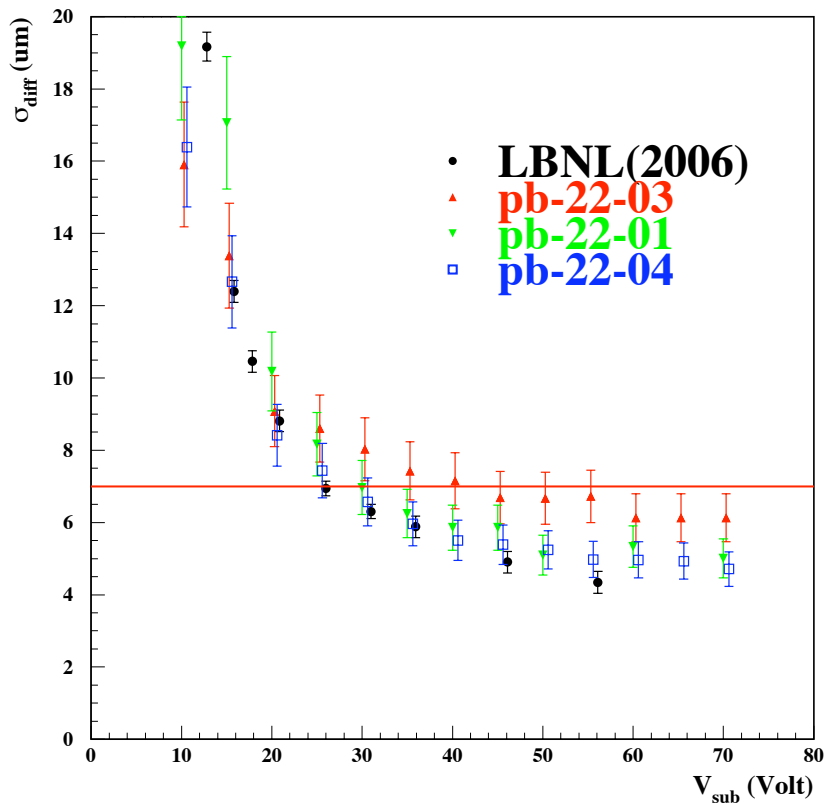


FIG. 21: Result of dispersion due to charge diffusion measured for three 2k x 2k CCD from the engineering production run for DECam. The plot also shows the results obtained in previous work [8] using the “spot machine” on similar devices. The LBNL measurements presented here were done for a 200  $\mu\text{m}$  thick CCD, the DECam CCDs are 250  $\mu\text{m}$  thick.

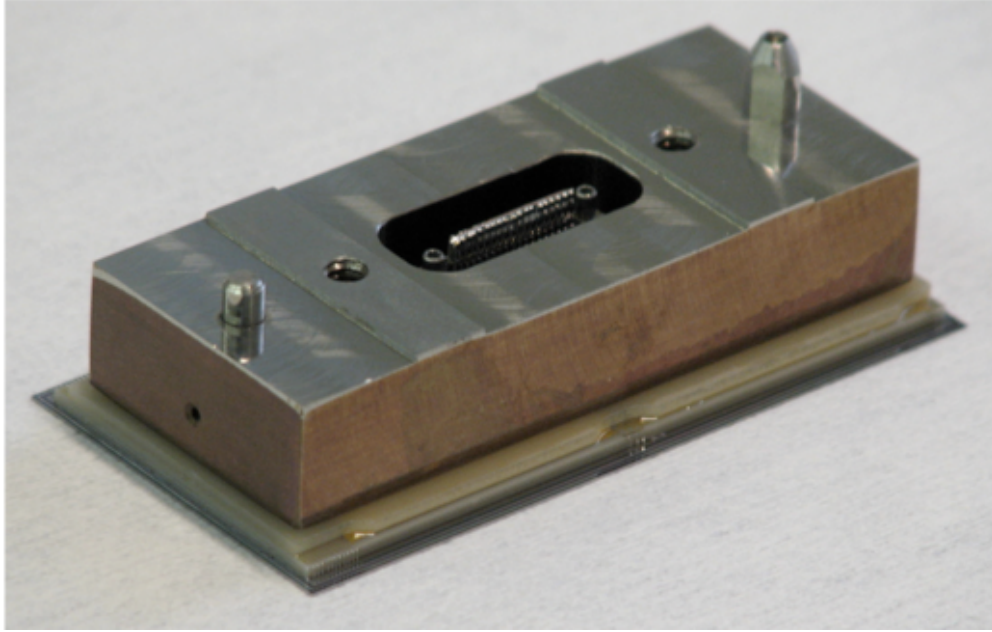


FIG. 22: Complete module showing CCD, AIN readout board, AIN spacer, and Invar foot. A temporary shorting plug inserted into the connector is visible. For details see Ref. [14].

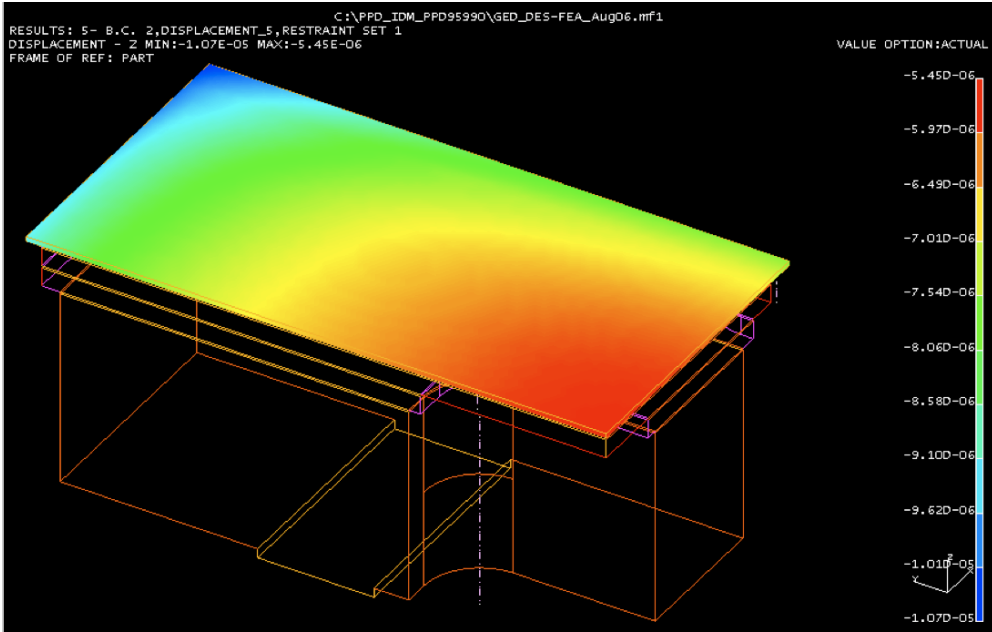


FIG. 23: Finite Element Analysis of flatness for the imaging surface of the DECcam science packages. A maximum thermal distortion of 5.2 μm is seen in this study.

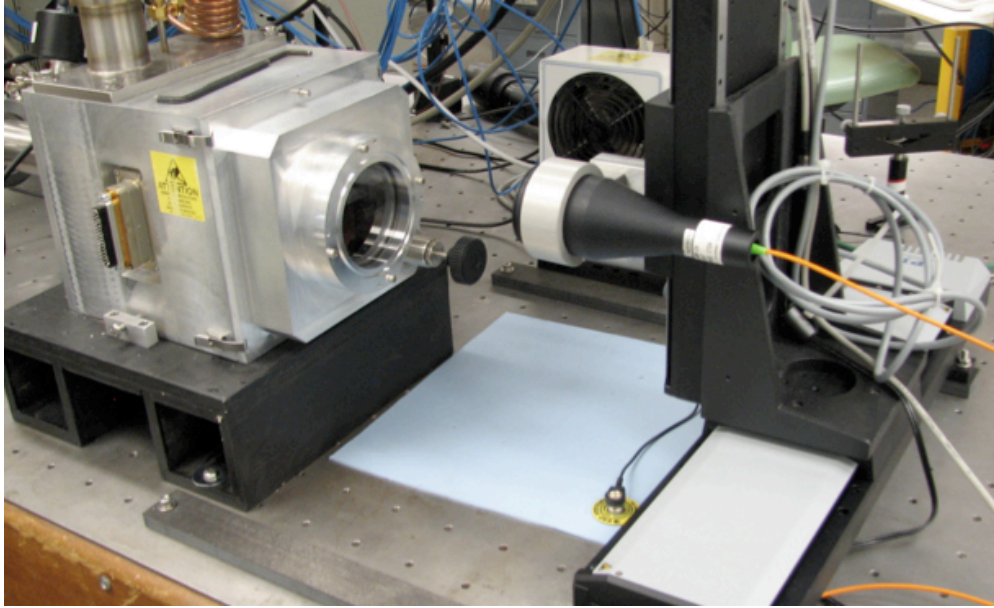


FIG. 24: Flatness setup in front of the CCD testing dewar.

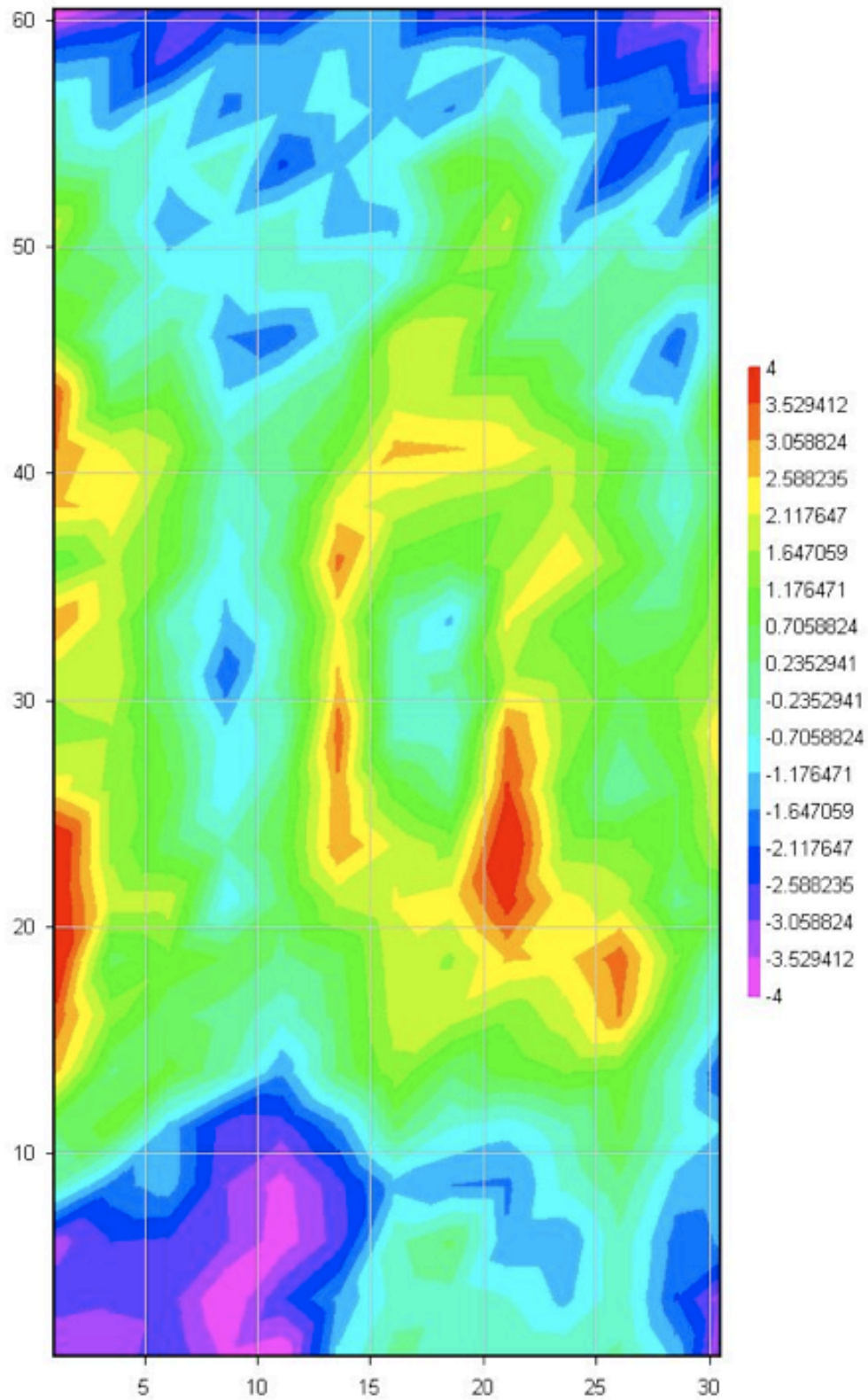


FIG. 25: Flatness measurement results for DECam prototype science package at 173 K.

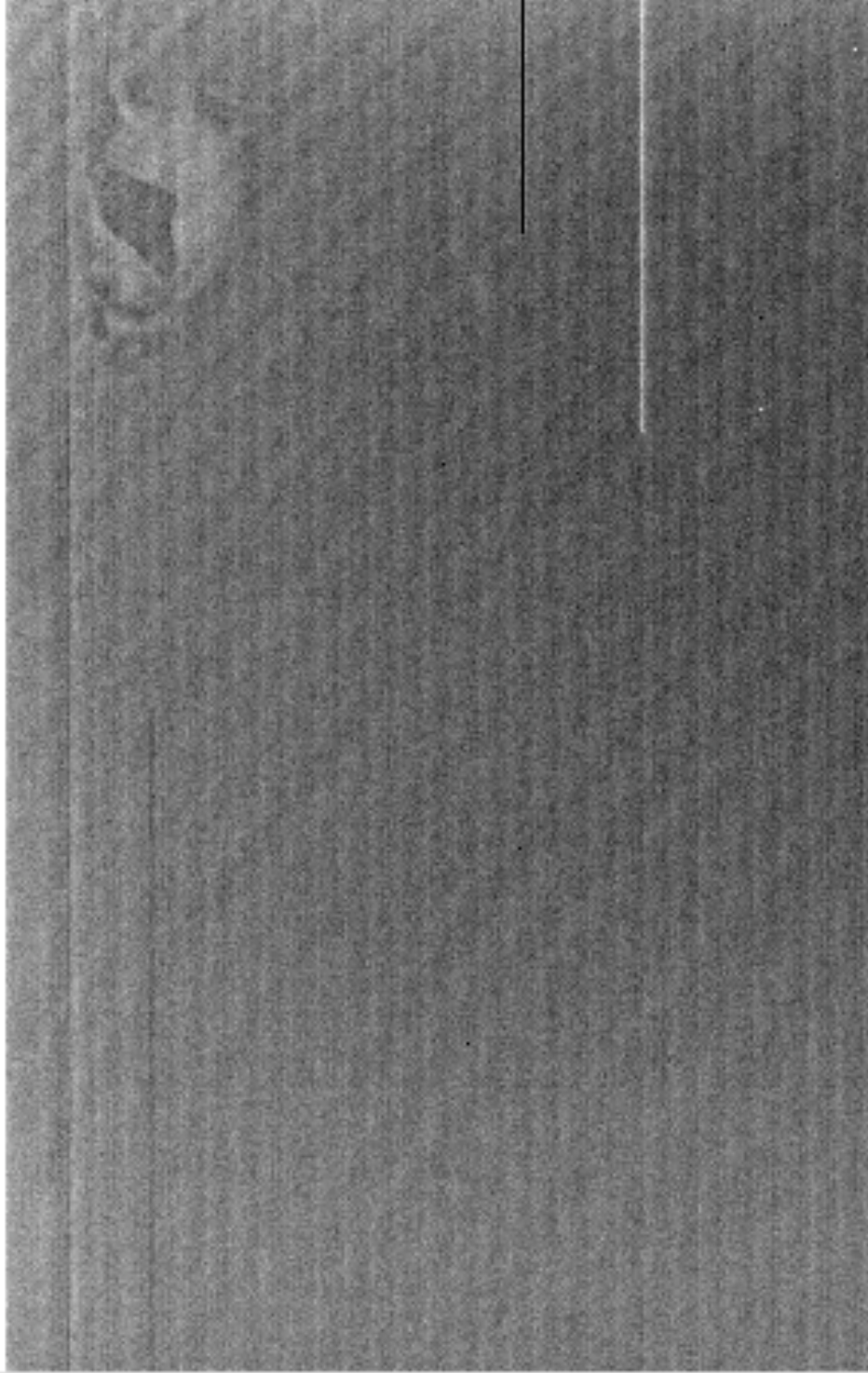


FIG. 26: Median of 10 flat exposures for the LH side of pb-22-04.

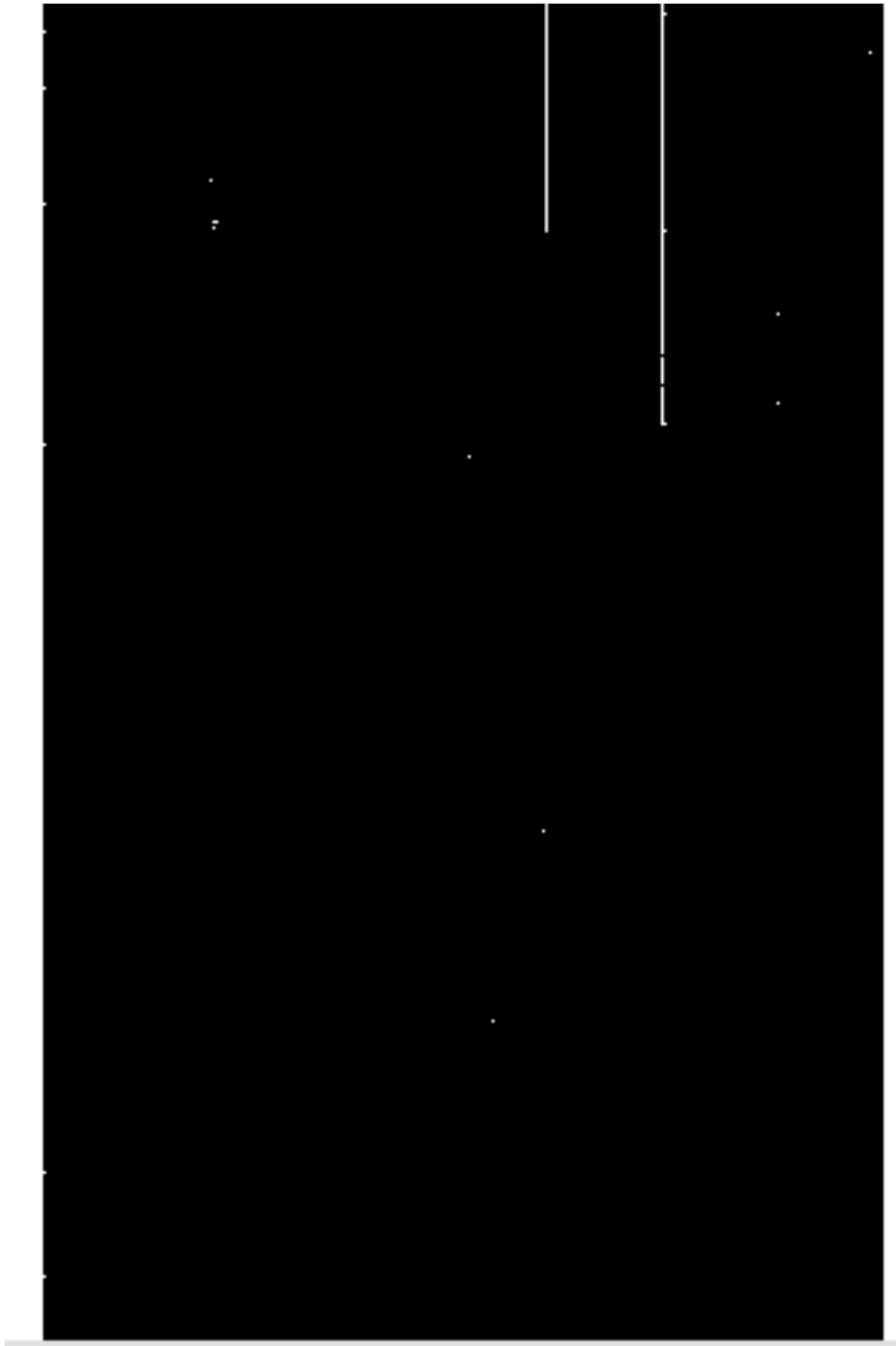


FIG. 27: Defects detected on Fig. 26.

defect size (pixels)	number of defects	area (pixels)	fraction (%)
+5% LH			
1	365	365	0.023
2-5	281	756	0.047
6-10	25	179	0.011
>10	41	2093	0.13
total	712	3393	0.21
-5% LH			
1	29	29	0.0018
2-5	6	17	0.0011
6-10	0	0	0.0
>10	2	779	0.048
total	37	825	0.051
total LH	749	4218	0.26
+5% RH			
1	43	43	0.0027
2-5	12	31	0.0019
6-10	1	7	0.00044
>10	19	19473	1.2
total	75	19554	1.2
-5% RH			
1	168	168	0.010
2-5	8	17	0.0011
6-10	0	0	0.0
>10	2	794	0.049
total	178	979	0.061
total RH	253	20533	1.3
total LH+RH	1047	24751	0.78

TABLE IV: Cosmetic defects detected on pb-22-04. The area affected by defective pixels is 0.78 % of the total number of pixels.

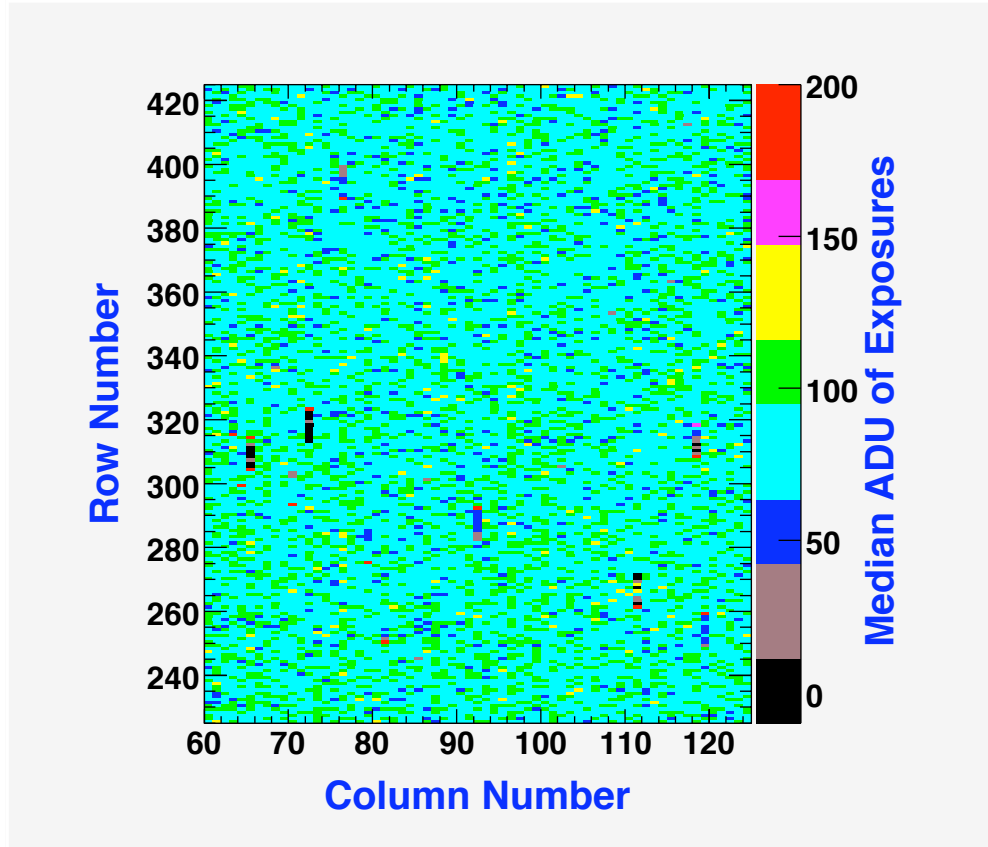


FIG. 28: Traps observed in a DECcam engineering CCD after irradiation in the Fermilab Neutron Facility. The traps are detected as dark vertical lines 10 pixels long with a brighter pixel at the edge as expected with pocket pumping.

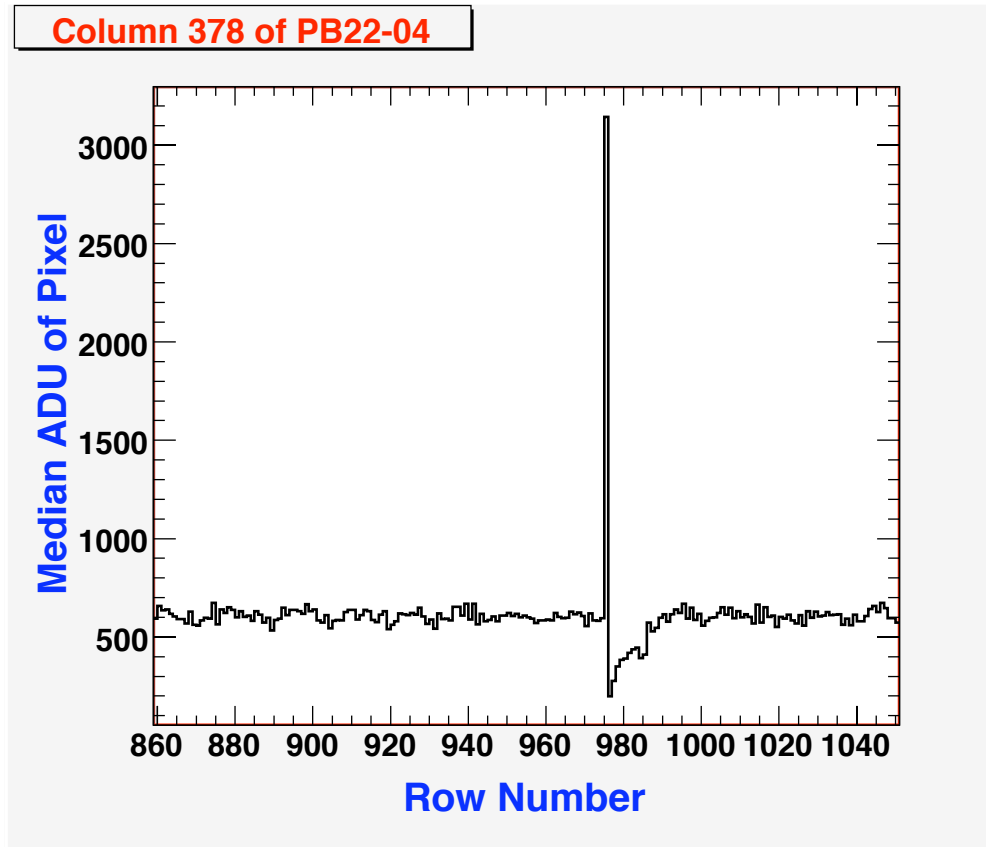


FIG. 29: Example of a trap detected using pocket pumping in a DECam engineering CCD from Lot 1B (pb-22-04).

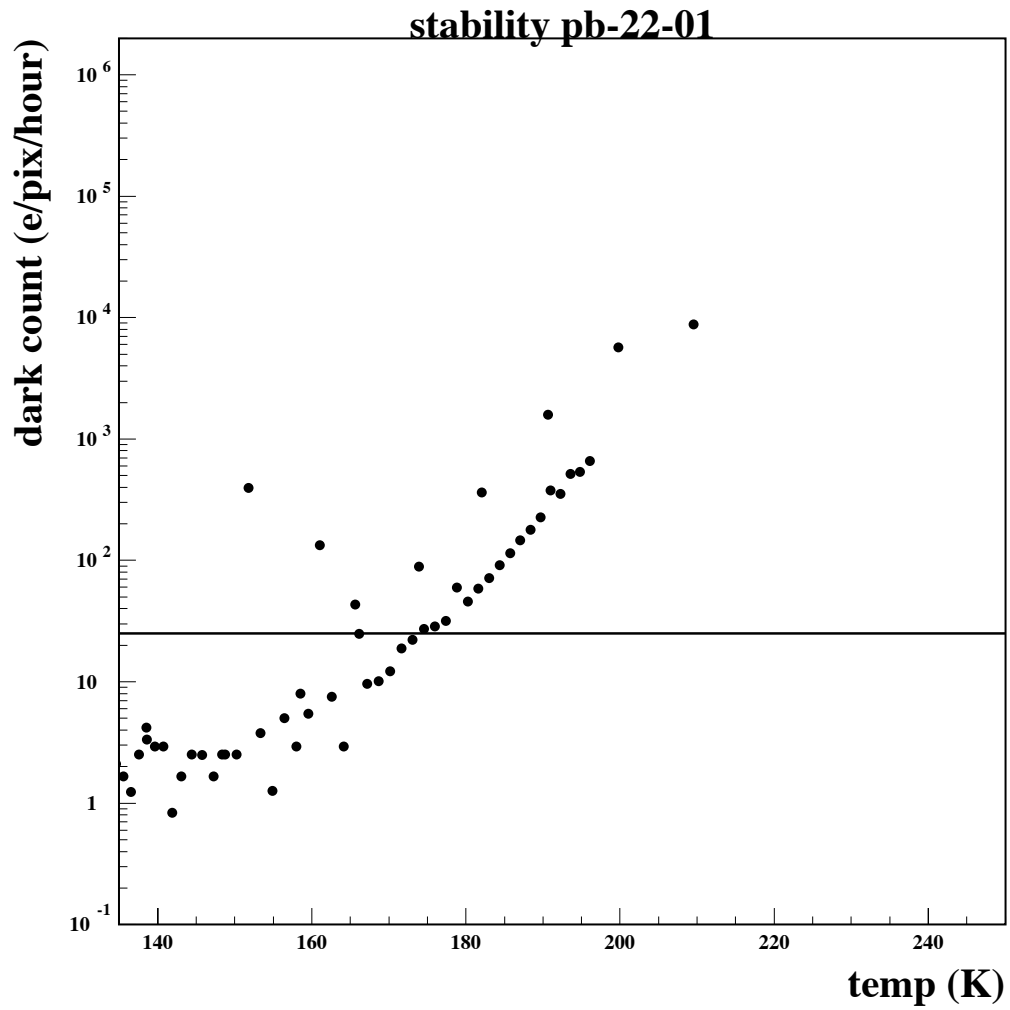


FIG. 30: Dark current as a function of temperature

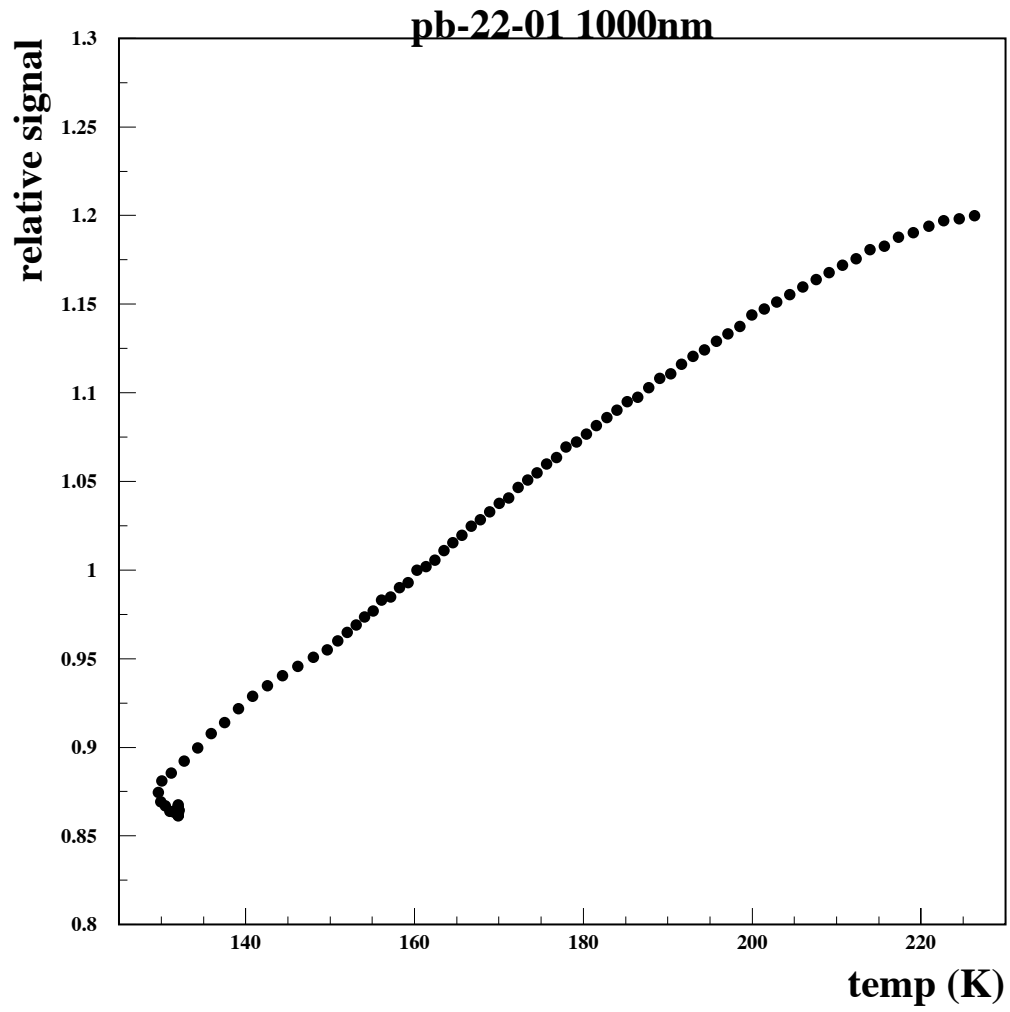


FIG. 31: relative QE at 1000nm as a function of temperature

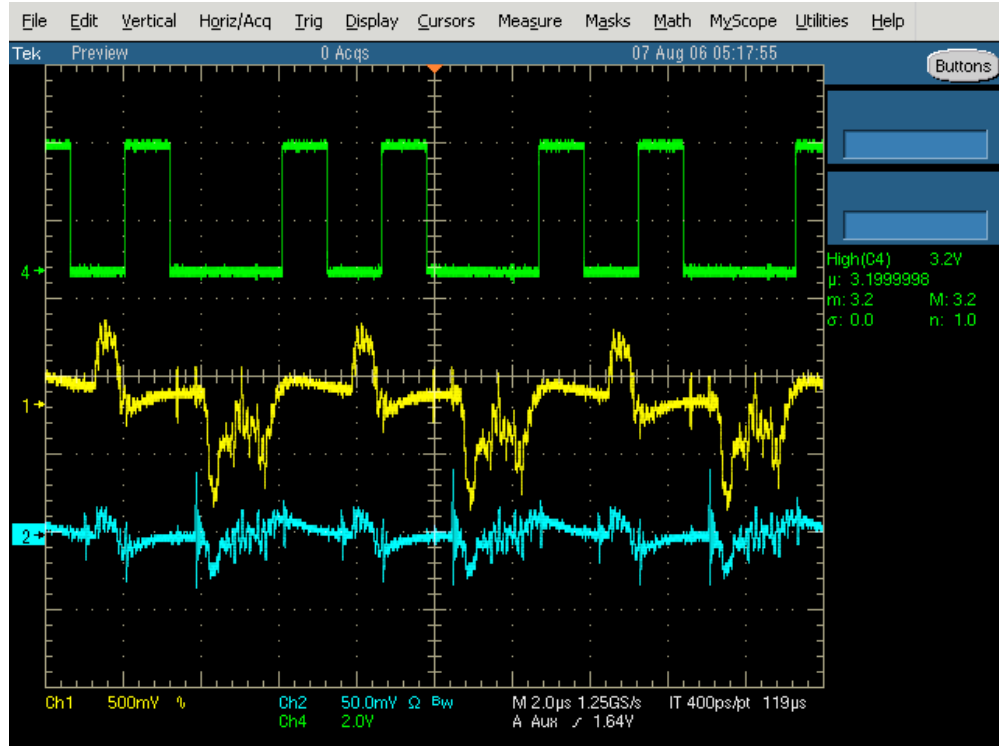


FIG. 32: Measured crosstalk on the readout electronics. The top trace shows the integration window used for the correlated double sampling of the video signal. The middle trace shows the video output of the CCD and the bottom trace shows the signal seen by the neighbor electronics channel. The scale for the signal trace is 10 times larger than for the crosstalk channel. The horizontal scale is  $2 \mu\text{sec}$  per division. Details are discussed in Ref. [11].

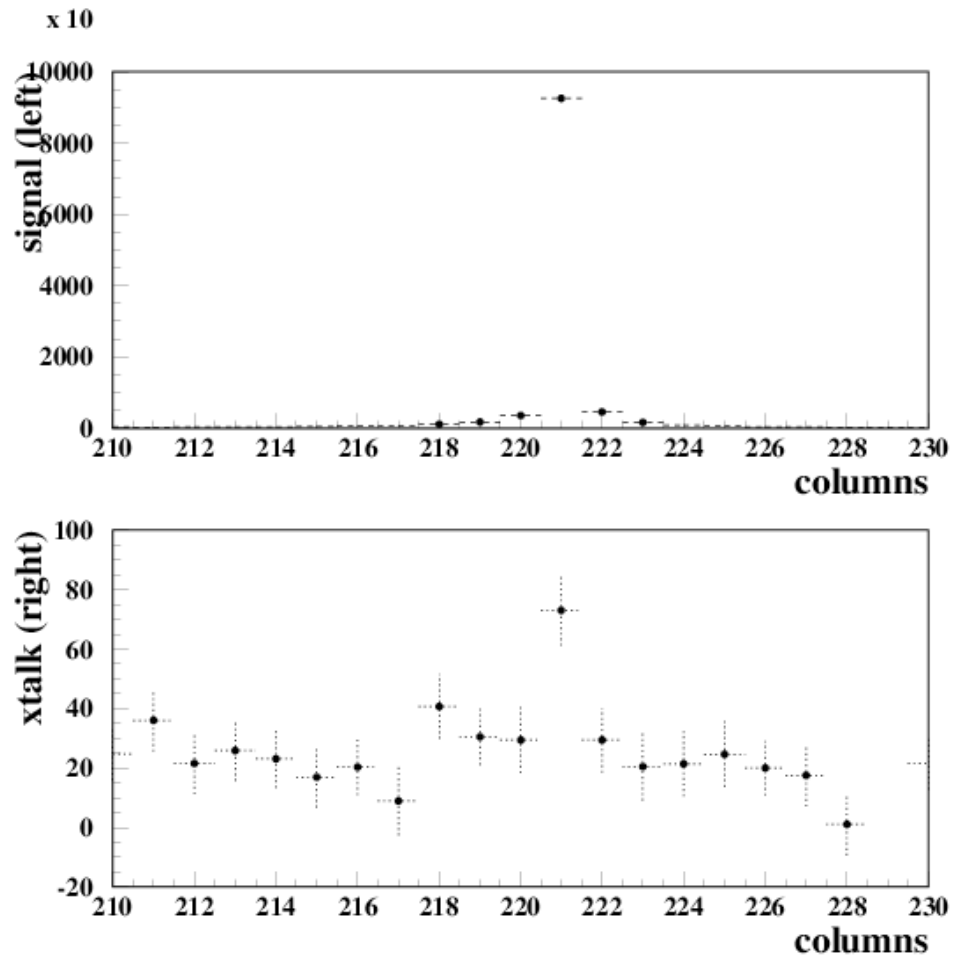


FIG. 33: Crosstalk measured between the two CCD channels. The upper panel shows a hot column seen on the left side of our CCD. The bottom panel shows the effect that the hot column has in the right channel. The ratio in the amplitude of the two peaks corresponds to the measured crosstalk of  $X_{CCD} = 7 \times 10^{-4}$ .